Geosci. Model Dev. Discuss., doi:10.5194/gmd-2015-266, 2016
Manuscript under review for journal Geosci. Model Dev.
Published: 19 January 2016

Geoscientific Model Development Discussions

Sensitivity of biogenic volatile organic compounds (BVOCs) to land surface parameterizations and vegetation distributions in California

[1]Chun Zhao, [1]Maoyi Huang, [1]Jerome D. Fast, [1]Larry K. Berg, [1]Yun Qian, [2]Alex Guenther, [2]Dasa Gu, [1]Manish Shrivastava, [1]Ying Liu, [3]Stacy Walters, [3]Gabriele Pfister, [4]Jiming Jin, [1]John E. Shilling, [5,6]Carsten Warneke

[1]*Atmospheric Science and Global Change Division, Pacific Northwest National Laboratory, Richland, WA, USA*

[2]*Department of Earth System Science, University of California, Irvine, California, USA*

[3]*National Center for Atmospheric Research, CO, USA*

[4]*Departments of Watershed Sciences and Plants, Soils, and Climate, Utah State University, Logan, UT, USA*

[5]*National Oceanic and Atmospheric Administration, Earth System Research Laboratory, USA*

[6]*CIRES, University of Colorado, Boulder, CO, USA*

Manuscript for submission to *WRF-Chem special issue in Geosci. Model Dev.*

*Corresponding author: Chun Zhao, phone: (509) 371-6372; email: chun.zhao@pnnl.gov

Geosci. Model Dev. Discuss., doi:10.5194/gmd-2015-266, 2016
Manuscript under review for journal Geosci. Model Dev.
Published: 19 January 2016

Geoscientific Model Development Discussions

Abstract. Current climate models still have large uncertainties in estimating biogenic trace gases, which can significantly affect atmospheric chemistry and secondary aerosol formation that ultimately influences air quality and aerosol radiative forcing. These uncertainties result from many factors, including uncertainties in land-surface processes and specification of vegetation types, both of which can affect the simulated near-surface fluxes of biogenic volatile organic compounds (BVOCs). In this study, the latest version of Model of Emissions of Gases and Aerosols from Nature (MEGAN v2.1) is coupled within the land surface parameterization CLM4 in the Weather Research and Forecasting model with chemistry (WRF-Chem). In this implementation, MEGAN v2.1 shares a consistent vegetation map with CLM4 for estimating BVOC emissions. This is unlike MEGAN v2.0 in the public version of WRF-Chem that uses a standalone vegetation map that differs from what is used by land surface parameterizations. This improved modeling framework is used to investigate the impact of two land surface parameterizations, CLM4 and Noah, on BVOCs and examine the sensitivity of BVOCs to vegetation distributions in California. The measurements collected during the Carbonaceous Aerosol and Radiative Effects Study (CARES) and the California Nexus of Air Quality and Climate Experiment (CalNex) conducted in June of 2010 provide an opportunity to evaluate the simulated BVOCs. Sensitivity experiments show that land surface parameterizations do influence the simulated BVOCs, but the impact is much smaller than that of vegetation distributions. This study indicates that more effort is needed to obtain the most appropriate and accurate land cover datasets for climate and air quality models in terms of simulating BVOCs, oxidant chemistry, and consequently secondary organic aerosol formation.

Geosci. Model Dev. Discuss., doi:10.5194/gmd-2015-266, 2016
Manuscript under review for journal Geosci. Model Dev.
Published: 19 January 2016

1. Introduction

Volatile organic compounds (VOCs) in the atmosphere play an important role in atmospheric chemistry, and therefore can significantly affect ozone and secondary organic aerosol (SOA) formation and ultimately air quality and climate [e.g., Chameides et al., 1992; Fehsenfeld et al., 1992; Andreae and Crutzen, 1997; Pierce et al., 1998; Poisson et al., 2000; Sanderson et al., 2003; Claeys et al., 2004; Arneth et al., 2010]. Significant effort has been made on obtaining accurate predictions of atmospheric VOC concentrations; however, there remain large differences between observed and simulated values. These uncertainties result from many factors, including biogenic emission rates that are influenced by near-surface meteorological processes, sub-surface processes, representation of vegetation distributions, and plant biology [Guenther et al., 2013].

Biogenic emissions are a major source of VOCs [e.g., Zimmerman et al., 1978; Mueller, 1992] in the atmosphere. In particular, isoprenoids (consisting mainly of isoprene and monoterpenes) that dominate biogenic VOCs (BVOCs) have been extensively investigated during the last five decades [e.g., Went, 1960; Rasmussen, 1972; Zimmerman et al., 1979; Lamb et al., 1987; Pierce et al., 1998; Niinemets et al., 1999 and 2002; Arneth et al., 2007; Schurgers et al., 2009; Guenther et al., 1995 and 2012]. BVOC emissions were originally computed offline, producing prescribed emission inventories used by regional and global models [e.g., Huang et al., 2011]. However, emissions of BVOCs depend on diurnal, multi-day, and seasonal variations in light intensity, temperature, soil moisture, vegetation type, and leaf area index (LAI) [e.g., Pierce et al., 1998; Niinemets et al., 1999 and 2002; Arneth et al., 2007; Schurgers et al., 2009; Guenther et al., 2012]. Therefore, various BVOCs emission algorithms have been

Geosci. Model Dev. Discuss., doi:10.5194/gmd-2015-266, 2016
Manuscript under review for journal Geosci. Model Dev.
Published: 19 January 2016

proposed that extrapolate limited laboratory and field measurements to prescribed regional and global ecosystems [e.g., Pierce et al., 1998; Niinemets et al., 1999 and 2002; Arneth et al., 2007; Schurgers et al., 2009; Guenther et al., 1995 and 2012]. The uncertainties in biogenic emission parameterizations are mainly due to the scarcity of observations of BVOCs fluxes and vegetation distributions over regional scales. Inappropriate coupling strategies between biogenic emission and land-surface parameterizations may also introduce errors in estimating atmospheric BVOCs. For example, some models specify different vegetation distributions for biogenic emissions and land-atmosphere interaction processes as applied in different parts of models.

BVOCs play a significant role in affecting the air quality and regional climate over California, where there have been many studies, such as the Carbonaceous Aerosol and Radiative Effects Study (CARES) [Zaveri et al., 2012] and the California Nexus of Air Quality and Climate Experiment (CalNex) [Ryerson et al., 2013], investigating the impacts of BVOCs and their interaction with anthropogenic pollutants. In the past 20 years, California's economy has grown rapidly and the population has increased by 33% [Cox et al., 2009]. Although California has reduced the emissions of most primary pollutants, poor air quality still affects the well-being of millions of people. Nearly all Californians live in areas that are designated as nonattainment for the state (about 99%) and national (about 93%) health-based O_3 and/or PM standards. Accurate predictions of O_3 and PM concentrations are needed to develop effective attainment strategies, but this is complicated, in part, due to uncertainties associated with long-range transport of pollutants and local natural emission sources such as BVOCs.

In California, the complex topography and distribution of vegetation makes it

Geosci. Model Dev. Discuss., doi:10.5194/gmd-2015-266, 2016
Manuscript under review for journal Geosci. Model Dev.
Published: 19 January 2016

93 difficult for models to capture the variability of BVOCs at regional and local scales. For
94 example, Fast et al. [2014] showed that simulated biogenic emissions varied by as much
95 as a factor of 2 within 8 km of an observation site in Cool, California. They also found
96 that daytime mixing ratios of isoprene and monoterpenes from a regional simulation
97 using the Weather Research and Forecasting model with chemistry (WRF-Chem) [Grell
98 et al., 2005; Fast et al., 2006] are usually a factor of two smaller than the observations
99 collected both at the rural Cool site and an urban Sacramento site. Conversely, simulated
100 monoterpene mixing ratios were similar to observations during the day but a factor of
101 three too high at night at the observation site in Cool. They suggested that the biogenic
102 emission rates calculated based on the Model of Emissions of Gases and Aerosols from
103 Nature version 2.0 (MEGAN v2.0) might contribute to major biases in their simulations.
104 Knote et al. [2014] also found that their simulations using WRF-Chem with MEGAN
105 v2.0 produced BVOCs concentrations that were too small over Los Angeles, and
106 suggested that there might be deficiencies in the description of vegetation in urban areas.
107 Thus, it is evident that uncertainties in simulated atmospheric BVOCs can arise from how
108 well vegetation is represented in models. Furthermore, to our knowledge, none of the
109 numerous chemical transport modeling studies for California have investigated the
110 sensitivity of BVOC simulations to land surface parameterizations and vegetation
111 distributions.

112 To better understand the uncertainties in simulating BVOCs associated with land
113 surface parameterizations and vegetation distributions in California, the latest version of
114 MEGAN (MEGAN v2.1) is coupled into the CLM4 land surface parameterization of
115 WRF-Chem in this study. Multiple sensitivity experiments are conducted using this

Geosci. Model Dev. Discuss., doi:10.5194/gmd-2015-266, 2016
Manuscript under review for journal Geosci. Model Dev.
Published: 19 January 2016

improved modeling framework at a relatively high spatial resolution to capture the region's complex topography and vegetation distribution. Simulations are conducted using WRF-Chem with "fully" coupled version of CLM4 and MEGAN v2.1 (i.e., CLM4 and MEGAN share a consistent vegetation dataset) and compared with the measurements collected during CARES and CalNex conducted in June 2010. This new coupling also adds the capability of quantifying the impact of different vegetation distributions on simulating BVOCs. Simulations are also performed using two land surface parameterizations (Noah and CLM4) coupled with MEGAN v2.0. As with previous studies using WRF-Chem, MEGAN v2.0 uses a different vegetation dataset from the land surface parameterizations. The WRF-Chem experiments with MEGAN v2.0 and MEGAN v2.1 are included together here as a reference for future studies in the community and for users interested in migrating from the widely used v2.0 to v2.1.

The rest of manuscript is organized as follows. Sections 2 and 3 describe the WRF-Chem model and the observations used in this study, respectively. The sensitivity of modeling BVOCs to the land surface schemes and the vegetation distributions are analyzed in section 4. The findings are then summarized and discussed in section 5.

2. Model Description and Experimental Design

2.1 WRF-Chem

The WRF-Chem (v3.5.1) configuration is similar to that used by Fast et al. [2014] for studying aerosol evolution over California, except that this study excludes aerosols and focuses on simulated BVOCs. The model includes numerous options for the treatment of physics and chemistry processes. In this study, the SAPRC-99

Geosci. Model Dev. Discuss., doi:10.5194/gmd-2015-266, 2016
Manuscript under review for journal Geosci. Model Dev.
Published: 19 January 2016

photochemical mechanism [Carter, 2000a,b] is selected to simulate gas-phase chemistry, and the Fast-J parameterization [Wild et al., 2000] for photolysis rates. For all the simulations in this study, we use the Yonsei University (YSU) parameterization [Hong et al., 2006] for the planetary boundary layer (PBL), the Monin-Obukhov similarity theory [Paulson, 1970] to represent the surface layer, the Morrison two-moment parameterization [Morrison et al., 2009] for cloud microphysics, the Kain-Fritsch parameterization [Kain 2004] for sub-grid scale clouds and precipitation, the RRTMG parameterization for longwave and shortwave radiation [Iacono et al., 2008]. Since Fast et al. [2014] has evaluated the simulated meteorological fields and gases and aerosols with a similar model configuration, this study will focus primarily on the BVOCs simulation.

2.2 Land surface parameterizations

Two land surface parameterizations, Noah and CLM4.0, are used to quantify how differences in the treatment of land surface processes, including latent and sensible heat fluxes, soil moisture, and surface albedo, affect near-surface meteorological conditions and consequently simulated BVOC emissions and concentrations. The Noah land surface parameterization, described by Barlage et al. [2010] and LeMone et al. [2010a, 2010b], has been used in numerous studies with WRF-Chem. Noah has four soil layers, with a total depth of two meters and a single slab snow layer lumped with the top-soil layer, which is set to a depth of 10 cm. Noah does not treat sub-grid scale variability within a model grid cell.

The Community Land Model version 4.0 (CLM4) [Lawrence et al. 2011; Jin et al., 2012] was recently coupled and released with WRF (since v3.5) as one of the land

Geosci. Model Dev. Discuss., doi:10.5194/gmd-2015-266, 2016
Manuscript under review for journal Geosci. Model Dev.
Published: 19 January 2016

surface parameterization options. CLM4 in global and region applications has been shown to be accurate in describing snow, soil, and vegetation processes [Zeng et al., 2002; Jin and Miller, 2007; Zhao et al., 2014]. CLM4 includes five layers for snow, 10 layers for soil, and a single-layer for vegetation. The soil is divided into 19 categories defined according to percentages of sand and clay. The two-stream approximation [Dickinson, 1983] is applied to vegetation when calculating solar radiation reflected and absorbed by the canopy as well as radiation transfer within the canopy. Each model grid cell can be divided into a maximum of 10 smaller cells to account for sub-grid scale heterogeneity and its impact on the land surface processes. The 24 United States Geological Survey (USGS) land use types are mapped to the 16 plant functional types (PFT's) in CLM4 based on a lookup table derived from Bonan et al. [1996]. Additional technical details of CLM4 are provided in Oleson et al. [2004].

2.3 MEGAN and coupling with CLM4

MEGAN is a modeling framework for estimating fluxes of biogenic compounds between terrestrial ecosystems and the atmosphere using simple mechanistic algorithms to account for the major known processes controlling biogenic emissions [Guenther et al., 2006, 2012]. Two versions (v2.0 and v2.1) of MEGAN are used in this study. MEGAN v2.1 is an update from MEGAN v2.0 [Guenther et al., 2006; Sakulyanontvittaya et al., 2008] that includes additional compounds, emission types, and controlling processes. MEGAN v2.1 estimates emissions (F_i) for 19 compound classes (i) from terrestrial landscapes based on emission factors ($\varepsilon_{i,j}$) at standard conditions for vegetation type j with fractional grid box areal coverage χ_j, i.e., $F_i = \gamma_i \Sigma \varepsilon_{i,j} \chi_j$, where γ_i is emission activity factor from the processes controlling emission responses to environmental and

Geosci. Model Dev. Discuss., doi:10.5194/gmd-2015-266, 2016
Manuscript under review for journal Geosci. Model Dev.
Published: 19 January 2016

phenological conditions [Guenther et al., 2006, 2012].

For emission factors, MEGAN v2.0 enabled users to customize vegetation emission type schemes ranging from detailed (e.g. individual plant species or sub species) to generic (e.g. a few broad vegetation categories). MEGAN2.1 emission factors can be specified from gridded maps based on species composition and species-specific emission factors or by using PFT distributions and the PFT specific emission factors. MEGAN2.0 defined emission factors as the net flux of a compound into the atmosphere, while MEGAN2.1 emission factor represents the net primary emission that escapes into the atmosphere but is not the net flux because it does not include the downward flux of chemicals from above canopy.

The publically available version of WRF-Chem includes the MEGAN v2.0 parameterization for calculating BVOC emission fluxes (WRF-Chem user guide: http://ruc.noaa.gov/wrf/WG11/Users guide.pdf). It has been widely used for gas and aerosol simulations [e.g., Shrivastava et al., 2011, 2013; Gao et al., 2011, 2014; Knote et al., 2014; Fast et al., 2014]. However, MEGAN v2.0 was originally not coupled into the land surface scheme in WRF-Chem (since v3.1), and used the climatological monthly mean surface air temperature and solar radiation to represent the values for last few days for biogenic emission calculation that needs both instantaneous values and mean values of past days of surface temperature and solar radiation. Figure 1 shows the example of the comparison between the input climatological and model simulated monthly mean surface air temperature in June. It is apparent that the monthly-averaged simulated surface air temperature is much different from the climatology value. In addition, the vegetation dataset (referred to as VEG-M, will be discussed in Section 2.4) used in MEGAN v2.0

Geosci. Model Dev. Discuss., doi:10.5194/gmd-2015-266, 2016
Manuscript under review for journal Geosci. Model Dev.
Published: 19 January 2016

for calculating BVOC emission fluxes is also different from the one used by the land surface parameterization, which allows MEGAN v2.0 to be used with any of the available land surface parameterizations in WRF-Chem. This inconsistency in vegetation distributions may introduce errors in simulating emissions and concentrations of BVOC. To avoid this inconsistency, we have coupled MEGAN v2.1 with WRF-Chem embedded in the CLM4 land surface parameterization. Therefore, the coupling of MEGAN v2.1 and CLM4 in WRF-Chem now has the same functionality as CLM4 in the Community Earth System Model (CESM) [Lawrence et al. 2011]. With this coupling strategy, MEGAN also uses the same vegetation dataset (i.e., 16 PFT's converted from the USGS dataset as discussed in Section 2.2) that CLM4 uses for all other land surface processes; this means, however, that MEGAN v2.1 can only be used with CLM4 in WRF-Chem. In addition, MEGAN v2.1 can compute BVOC emissions that account for the sub-grid variability of vegetation distributions within CLM4.

2.4 Vegetation datasets

As mentioned previously, the first 16-PFT dataset (referred to as USGS hereafter) used by CLM4 is converted from the default 24 USGS land cover dataset used by WRF-Chem based on a lookup table derived from Bonan et al. [1996]. This method is also applied to three other 16-PFT's datasets (referred to as VEG1, VEG2, and VEG3) used by CLM4 in WRF-Chem. The sensitivity of simulating BVOC emissions by CLM4 to these four 16-PFT's datasets is quantified. The VEG1, VEG2, and VEG3 datasets are derived from different sources as described next.

The VEG1 dataset is from the PFT fractional cover product by Ke et al. [2012], which was developed from the Moderate Resolution Imaging Spectroradiometer

Geosci. Model Dev. Discuss., doi:10.5194/gmd-2015-266, 2016
Manuscript under review for journal Geosci. Model Dev.
Published: 19 January 2016

(MODIS) PFT classifications for the year 2005 for determining seven PFTs including needleleaf evergreen trees, needleleaf deciduous trees, broadleaf evergreen trees, broadleaf deciduous trees, shrub, grass and crop for each 500 m pixel. The WorldClim 5 arc-minute (0.0833°) [Hijmans et al., 2005] climatological global monthly surface air temperature and precipitation data was interpolated to a 500 m grid and used to further reclassify the PFTs into 15 PFTs, and fractions of crop grasses were mapped based on the method presented in Still et al. [2003]. Pixels with barren land and urban areas were reassigned to the bare soil class. The bare soil and the 15 PFTs from the 500-m grid were then aggregated to a 0.05° grid.

The VEG2 dataset is obtained from the NCAR CESM data repository [Oleson et al., 2010], available on a 0.05^{o} grid and derived using a combination of the 2001 MODIS Vegetation Continuous Field (VCF), MODIS land cover product for year 2000 [Lawrence and Chase, 2006; Lawrence and Chase, 2007], and 1992-1993 AVHRR Continuous Field Tree Cover Project data [Lawrence and Chase, 2007; Lawrence et al., 2011]. The monthly surface air temperature and precipitation data from Willmott and Matsuura [2001] was used to further reclassify the seven PFTs into bare soil and 15 PFTs in the tropical, temperate and boreal climate groups based on climate rules described by Bonan et al. [2002]. Fractions of crop grasses were mapped based on the method presented in Still et al. [2003].

The VEG3 dataset is derived from a high-resolution (30 arc-second) dataset over the U.S. with 16 PFT classifications for the year 2008. The dataset was created by combining the National Land Cover Dataset (NLCD, Homer et al., 2004) and the Cropland Data Layer (see http://nassgeodata.gmu.edu/CropScape/), both of which were

Geosci. Model Dev. Discuss., doi:10.5194/gmd-2015-266, 2016
Manuscript under review for journal Geosci. Model Dev.
Published: 19 January 2016

based on the 30-m LANDSAT-TM satellite data. Vegetation species composition information was obtained from the Forest Inventory and Analysis (see http://www.fia.fs.fed.us) and the soil data from the Natural Resources Conservation Services (see http://sdmdataaccess. nrcs.usda.gov/). The processing included adjusting the NLCD tree cover estimates in urban areas to account for the substantial underestimation of trees in the LANDSAT-TM data [Duhl et al., 2012]. This was accomplished using the regionally specific adjustment factors for urban NLCD developed by Greenfield et al. [2009] using the high-resolution imagery.

Figure 2 shows the spatial distributions of the dominant PFT in each 4×4 km^2 grid cell of the simulation domain from each of the four datasets. Not only are the grid-dominant PFTs very different among the four datasets, but the sub-grid distributions of PFTs are different as well (not shown). The domain-averaged fractions of 16 PFTs from the four datasets listed in Table 1 also illustrate the differences in PFT distributions. For example, the fraction of temperate broadleaf deciduous tree ranges from 0.4% in VEG1 to 1.8% in VEG2 and the fraction of temperate broadleaf deciduous shrub ranges from 10.8% in VEG3 to 37.5% in VEG1. This difference in PFT distributions can affect the BVOC emission calculations. For example, Figure 3 shows the biogenic isoprene emission factor for each PFT prescribed in MEGAN v2.1 in CLM4. It shows that temperate broadleaf deciduous tree (PFT 7 listed in Table 1) has a large isoprene emission factor, while temperate needleleaf evergreen tree (PFT 1 listed in Table 1) has a small isoprene emission factor. Finally, the distribution of broadleaf tree, needleleaf tree, shrub, and herbaceous vegetation categories used by MEGAN v2.0 (refer to VEG-M) is shown in Figure 4. In MEGAN v2.0 of WRF-Chem, only these four PFT's are considered

Geosci. Model Dev. Discuss., doi:10.5194/gmd-2015-266, 2016
Manuscript under review for journal Geosci. Model Dev.
Published: 19 January 2016

for the biogenic emission calculation because they are the only ones included in the MEGAN v2.0 PFT scheme. As discussed previously, these are different from the USGS vegetation distribution used by Noah and CLM4 and may cause additional biases.

2.5 Numerical experiments

The simulations are performed using a domain encompassing California (Fig. 1) with a horizontal grid spacing of 4 km and 279×279 grid cells (113°W-128°W, 32°N-43°N) and 51 vertical layers up to 100 hPa with about 35 layers below 2 km. The simulation period is from May 25 to June 30 2010, but only the results in June are used for analysis to allow for the model to "spin-up" realistic distributions of trace gases. The initial and boundary conditions are prescribed by large-scale meteorological fields obtained from the North American Regional Reanalysis (NARR) data with updates provided at 6-h intervals, which also provide the prescribed sea surface temperature (SST) for the simulations. The modeled u-component and v-component wind and atmospheric temperature are nudged towards the NARR reanalysis data with a nudging time scale of 6 hours [Stauffer and Seaman, 1990]. Chemical lateral boundary conditions are from the default profiles in WRF-Chem, which are based on the averages of mid-latitude aircraft profiles from several field studies over the eastern Pacific Ocean [McKeen et al., 2002].

Anthropogenic emissions were obtained from the CARB 2008 ARCTAS emission inventory developed for the NASA Arctic Research of the Composition of the Troposphere from Aircraft and Satellite (ARCTAS) mission over California [Pfister et al., 2011]. The CARB inventory contains hourly emissions for a 13-day period using a 4-

Geosci. Model Dev. Discuss., doi:10.5194/gmd-2015-266, 2016
Manuscript under review for journal Geosci. Model Dev.
Published: 19 January 2016

km grid spacing over California. We created diurnally averaged emissions from 5 of the weekdays and 2 of the weekend days and used those averages for all weekdays and weekends and applied these over the entire simulation period. Anthropogenic emissions from the 2005 National Emissions Inventory (NEI) (WRF-Chem user guide from http://ruc.noaa.gov/wrf/WG11/Users guide.pdf) were used for regions outside of California. Biomass burning is not considered in the present study, because satellite detection methods indicated that there were very few fires in California during the simulation period. Biogenic emissions were computed on-line using the MEGAN model and lumped into isoprene, terpenes, and sesquiterpenes for the SAPRC-99 photochemical mechanism.

As discussed previously, multiple numerical experiments summarized in Table 2 are conducted with different combinations of land surface schemes and vegetation datasets to investigate the sensitivity of BVOCs simulation to land surface parameterizations and vegetation distributions. First, we conduct two experiments using MEGAN v2.0 coupled with the Noah (Mv20Noah) and CLM4 (Mv20CLM) land surface parameterizations, respectively. The Noah land surface scheme is only coupled with MEGAN v2.0 in WRF-Chem. In these two experiments, the two land surface parameterizations use the USGS vegetation distributions while MEGAN v2.0 uses a separate vegetation map (VEG-M) to estimate BVOCs emissions. By comparing these two experiments, the impact of land surface parameterizations on simulated BVOC concentrations are examined. Second, we conduct four experiments using MEGAN v2.1 embedded in the CLM4 land surface parameterization with four different vegetation datasets, i.e., USGS (Mv21USGS), VEG1 (Mv21V1), VEG2 (Mv21V2), and VEG3

Geosci. Model Dev. Discuss., doi:10.5194/gmd-2015-266, 2016
Manuscript under review for journal Geosci. Model Dev.
Published: 19 January 2016

(Mv21V3). The differences among these four experiments show the impact of vegetation distributions on simulated BVOC concentrations.

We note that MEGAN v2.0 and v2.1 use different vegetation datasets and are implemented in WRF-Chem in different ways, but the objective of this study is not to explore how the formulations of these two versions of MEGAN affect BVOC concentrations. The better way for exploring the version difference of MEGAN is to implement both versions in the same way and use the same vegetation dataset. The simulated BVOC emissions and concentrations by WRF-Chem with MEGAN v2.0 and MEGAN v2.1 are included together here as a reference for future studies in the community and for users interested in migrating from the widely used v2.0 to v2.1.

3. Observations

Measurements of VOCs collected by proton transfer reaction mass spectrometer (PTR-MS) instruments [Lindinger et al., 1998] and a gas chromatography instrument [Gentner et al., 2012] over California during June of 2010 as part of the CARES and CalNex campaigns are used to evaluate the simulated isoprene and monoterpene concentrations. CARES was designed to address science issues associated with the interactions of biogenic and anthropogenic precursors on SOA, black carbon mixing state, and the effects of organic species and aerosol mixing state on optical properties and the activation of cloud condensation nuclei [Zaveri et al., 2012]. As shown in Figure 5, ground-based instruments were deployed at two sites (T0 and T1) in northern California: T0 in Sacramento (38.649 °N, -121.349°W, ~ 30 m m.s.l., denoted by red upward triangle) and T1 in Cool (38.889°N, -120.974°W, ~ 450 m m.s.l., denoted by red

Geosci. Model Dev. Discuss., doi:10.5194/gmd-2015-266, 2016
Manuscript under review for journal Geosci. Model Dev.
Published: 19 January 2016

346 downward triangle), a small town located about 40 km northeast of Sacramento. The U.S.
347 Department of Energy (DOE) Gulfstream 1 (G-1) research aircraft sampled
348 meteorological, trace gas, and aerosol quantities aloft in the vicinity of the T0 and T1
349 sites, denoted by black lines in Figure 6. Zaveri et al. [2012] described the
350 instrumentation for each of the surface sites and Shilling et al. [2013] described VOC
351 measurements on the G-1. Most of the sampling during CARES occurred between 2 and
352 28 June, and only the aircraft sampling within 1 km of the surface is used to evaluate
353 model simulations because G-1 sampled below 1 km for the majority of time.

354 CalNex was designed to address science issues relevant to emission inventories,
355 dispersion of trace gases and aerosols, atmospheric chemistry, and the interactions of
356 aerosols, clouds, and radiation [Ryerson et al., 2013]. Ground-based instruments were
357 deployed at two sites in southern California as shown in Figure 5: one in Pasadena
358 (34.141°N, -118.112°W, ~240 m m.s.l., denoted by the red circle) and one in Bakersfield
359 (35.346°N, −118.965°W, ~ 123 m m.s.l., denoted by the red square). The NOAA WP-3D
360 research aircraft sampled meteorological, trace gas, and aerosol quantities aloft along
361 flight paths shown in Figure 5 (denoted by blue lines). While most of the CalNex aircraft
362 tracks below an altitude of 1 km were conducted in southern California in the vicinity of
363 the Los Angeles basin, the WP-3D also flew within the Central Valley and in the vicinity
364 of Sacramento on some days. A detailed description of the instrumentation for each of the
365 CalNex surface sites and mobile platforms is given by Ryerson et al. [2013]. Most of the
366 sampling during CalNex was conducted before June 16 and only the aircraft sampling
367 below 1 km is used to evaluate the model simulations.
368

Geosci. Model Dev. Discuss., doi:10.5194/gmd-2015-266, 2016
Manuscript under review for journal Geosci. Model Dev.
Published: 19 January 2016

4. Results

4.1 Impact of land surface schemes

4.1.1 Biogenic isoprene and monoterpene emissions

Figure 5 shows the spatial distributions of biogenic isoprene emissions averaged over June for the six simulations listed in Table 2. Biogenic isoprene emissions occur in vegetated regions of California with the highest emission rates along the foothills of the Sierra Nevada where oak trees are the dominant plant species. To show the difference in biogenic isoprene emissions among the cases more clearly, Figure 6a and 6b zoom in on the CARES (northern California) and CalNex (southern California) sampling regions, respectively. In both regions the differences in land surface parameterizations had a relatively small impact on the biogenic isoprene emissions over California in terms of both spatial distribution and magnitude, although the emissions from Mv20CLM were a little larger than those from Mv20Noah. The domain summed biogenic isoprene emissions for the entire month of June from Mv20Noah and Mv20CLM are 1.4×10^9 and 1.6×10^9 mole, respectively. Figure 7a and 7b are similar to Figure 6a and 6b, except that biogenic monoterpene emission fluxes are shown. In general, the spatial patterns of emissions of the two biogenic species are similar, except that the peak areas of monoterpene emissions are shifted slightly. For example, the peak monoterpene emissions in northern California occur further northeast at higher elevations of the Sierra Nevada that are dominated by needleleaf evergreen trees. The impact of land surface schemes on biogenic monoterpene emissions is also small over California in terms of both spatial patterns and magnitudes, although the emissions from Mv20CLM are a little larger than those from Mv20Noah. The domain summed biogenic monoterpene emissions

Geosci. Model Dev. Discuss., doi:10.5194/gmd-2015-266, 2016
Manuscript under review for journal Geosci. Model Dev.
Published: 19 January 2016

for the entire month of June from Mv20Noah and Mv20CLM are $1.0x10^8$ and $1.1x10^8$ mole, respectively.

The similarity in estimating biogenic emissions between the experiments with two land surface parameterizations is also summarized in Figures 8 and 9, which show the average diurnal biogenic isoprene and monterpene emission rates at the four observation sites. The similarity between Mv20Noah and Mv20CLM (red and orange lines) is likely due to the same vegetation map in MEGAN v2.0 to estimate biogenic emissions. Although the two land surface parameterizations produce some difference in surface temperature (Fig. 1), soil moisture (not shown), and net solar radiation near the surface (not shown), their impact on the biogenic emissions was small. Both BVOC species have peak emission rates in the early afternoon. One noteworthy difference in diurnal variation of the two biogenic species emission rates is that there is no isoprene emitted during the night while the amount of monoterpenes emitted during the night is small but not negligible. This can contribute to differences in the diurnal variation of the mixing ratios of two biogenic species, as will be discussed next.

4.1.2 Isoprene and monoterpene mixing ratios

Figures 10a,b and 11a,b show the spatial distributions of monthly-averaged surface mixing ratios of isoprene+MVK(methyl-vinylketone)+MACR(methacrolein) and monoterpenes, respectively, around the CARES (northern California) and the CalNex (central and southern California) sampling regions simulated by the six experiments listed in Table 2. Due to the fast chemical transition from isoprene to MVK and MACR, the sum of isoprene+MVK+MACR mixing ratios can better reflect the impact of biogenic isoprene emissions than isoprene mixing ratio alone [Shilling et al., 2013]. In

Geosci. Model Dev. Discuss., doi:10.5194/gmd-2015-266, 2016
Manuscript under review for journal Geosci. Model Dev.
Published: 19 January 2016

general, the spatial patterns and magnitudes of surface isoprene+MVK+MACR and monoterpene mixing ratios over the two regions are similar from the two MEGAN v2.0 experiments with the Noah and CLM4 land surface parameterizations, respectively. The spatial patterns of surface mixing ratios of isoprene+MVK+MACR and monoterpene are similar to the spatial variability in the emission rates.

There is difference between the two experiments at specific locations, which is partly reflected in the comparison of average diurnal variations of surface mixing ratios of isoprene+MVK+MACR and monoterpene at the four observation sites shown in Figure 12. Note that the values for the Bakersfield and Pasadena sites are averaged over the first two weeks of June to be consistent with the observations. Although both experiments with Noah and CLM4 (red and orange lines, respectively) simulate similar isoprene emission fluxes with the maximum in the afternoon (Fig. 8), their isoprene+MVK+MACR mixing ratios are different at the four sites, particularly at the site T0, where the Mv20CLM simulated isoprene+MVK+MACR mixing ratios during the daytime are about a factor of 2 larger than those from Mv20Noah. This difference mainly results from the difference in the near surface meteorology, such as net surface radiation and temperature, between the two experiments (not shown) that affects photochemistry. When compared to the observations, both experiments significantly underestimate the isoprene+MVK+MACR mixing ratios except at the Bakersfield site. Figure 13 is identical to Figure 12, except for surface monoterpene mixing ratios. Note that there were no monoterpene data reported for the Bakersfield and Pasadena sites, so only the simulation results are shown. In contrast to isoprene+MVK+MACR, monoterpenes exhibit peak surface mixing ratios during the nighttime due to the strong

Geosci. Model Dev. Discuss., doi:10.5194/gmd-2015-266, 2016
Manuscript under review for journal Geosci. Model Dev.
Published: 19 January 2016

438 photolysis activity that makes the lifetime of monoterpenes short during the daytime and
439 the small emissions into a shallow boundary layer during the nighttime (Fig. 9). In
440 general, the difference between the Mv20Noah and MV20CLM experiments in
441 monoterpene mixing ratios is relatively small at these four sites, particularly during the
442 daytime. When compared to the observations, both experiments overestimate the diurnal
443 variation and the nighttime surface monoterpene mixing ratios at the T0 and T1 sites.

444 Figures 14 and 15 show the comparison of the observed and simulated mixing
445 ratios of isoprene+MVK+MACR and monoterpene, respectively, along the G-1 and WP-
446 3D flight tracks below 1 km. Model results are sampled along the flight tracks. As shown
447 in Figure 5, the G-1 flight mainly flew over northern California around the T0 and T1
448 sites, while the WP-3D flew over a larger area covering both southern California and the
449 Central Valley. To better reflect the spatial variability in the BVOCs, the flight tracks of
450 both flights are separated into two regions as indicated by the black lines in Figure 10a,b
451 and Figure 11a,b. For the G-1, the flight paths are divided into regions of southwest and
452 northeast of the black line shown in Figures 10a and 11a that is parallel to the Sierra
453 Nevada. The two regions have significantly different vegetation (Fig. 2) resulting in large
454 differences in biogenic emissions. For the WP-3D, the flight paths are divided into
455 regions of south and north of the black line shown in Figures 10b and 11b to separate
456 southern California and the Central Valley. Over southern California, the measured
457 isoprene+MVK+MACR mixing ratios by the PTR-MS over the WP-3D are the upper
458 limit since the PTR-MS may have a small interference in urban areas for isoprene and
459 MVK+MACR.

460 In Figure 14, it is interesting to note that both experiments Mv20Noah and

Geosci. Model Dev. Discuss., doi:10.5194/gmd-2015-266, 2016
Manuscript under review for journal Geosci. Model Dev.
Published: 19 January 2016

461 Mv20CLM reasonably capture the variability seen in the G-1 isoprene+MVK+MACR
462 measurements over the southwest region even though they underestimate the surface
463 observations by as much as a factor of 2 at the T0 site (Fig. 12). While both experiments
464 are slightly smaller than observed, the Mv20CLM simulated mixing ratios are a little
465 larger than those from Mv20Noah and closer to the observations. Over the northeast
466 region, both experiments produced similar mixing ratios that were significantly smaller
467 than the observations, which is consistent with the comparison between the simulated and
468 observed isoprene+MVK+MACR at the T1 site (Fig. 12). As shown in Figure 14, the
469 Mv20CLM simulation produced somewhat larger isoprene+MVK+MACR mixing ratios
470 than Mv20Noah in both southern California and the Central Valley. This is consistent
471 with the comparison at the Bakersfield and Pasadena surface sites. Both simulations also
472 underestimate and overestimate the isoprene+MVK+MACR mixing ratios over southern
473 California and the Central Valley, respectively. The comparison of
474 isoprene+MVK+MACR with aircraft observations may suggest that both experiments
475 underestimate biogenic isoprene emissions over the forested foothills of Sierra Nevada
476 and southern California around Los Angeles, but overestimate the emissions over the
477 Central Valley. The model biases may also be affected, to some extent, by anthropogenic
478 emissions with large uncertainties and the associated non-linear chemistry due to the
479 mixing of anthropogenic and biogenic plumes [Fast et al., 2014].

480 Figure 15 shows that both experiments Mv20Noah and Mv20CLM significantly
481 underestimate the monoterpene mixing ratios over all the regions sampled by the G-1 and
482 WP-3D aircraft and that the differences between the simulations were negligible. The
483 average monoterpene mixing ratios sampled by the G-1 below 1 km was comparable to

Geosci. Model Dev. Discuss., doi:10.5194/gmd-2015-266, 2016
Manuscript under review for journal Geosci. Model Dev.
Published: 19 January 2016

the surface measurement at the T0 site during the daytime, but somewhat higher than the observations at the T1 site. The simulated mixing ratios averaged along the flight tracks were much smaller than those at the two surface sites, suggesting that it may be difficult for model to simulate the large spatial heterogeneity of the monoterpene mixing ratios. This could result from the biases in biogenic monoterpene emissions and/or the chemical mechanism for monoterpene oxidation and how chemistry is coupled with turbulent mixing within the simulated convective boundary layer. It also needs to be noted that the G-1 and WP-3D measured monoterpene mixing ratios are generally below the Limit Of Detection (LOD) of instruments (0.1-0.3 ppbv). Therefore, the true monoterpene mixing ratios could be range between 0 ~ 0.1-0.3 ppbv, which may also contribute to the discrepancy between observations and simulations.

4.2 Impact of vegetation distributions

4.2.1 Biogenic isoprene and monoterpene emissions

Figures 6a,b and 7a,b show that the differences in biogenic isoprene and monoterpene emission distributions due to using the various vegetation datasets are larger than the differences resulting from the two land surface parameterizations. The domain summed biogenic isoprene emissions for the entire month of June are 2.3, 0.76, 1.7, and 0.92 ($\times 10^9$ mole) from the experiments of Mv21USGS, Mv21V1, Mv21V2, and Mv21V3, respectively, and biogenic monoterpene emissions are 2.5, 1.7, 1.9, and 1.1 ($\times 10^8$ mole) from the four experiments, respectively. Each of the four simulations produces high biogenic isoprene and monoterpene emission rates along the Sierra Nevada that is covered mainly by oak and pine forests. However, the different forest

Geosci. Model Dev. Discuss., doi:10.5194/gmd-2015-266, 2016
Manuscript under review for journal Geosci. Model Dev.
Published: 19 January 2016

classifications and their coverage (Table 1) produce different biogenic isoprene and monoterpene emission rates along the Sierra Nevada. Another distinct difference among these four simulations is found over the Central Valley, where the Mv21V1 and Mv21V3 experiments produce significantly lower biogenic isoprene and monoterpene emissions than the Mv21USGS and Mv21V2 experiments. This results from their different spatial distributions of vegetation types. For example, the vegetation dataset in MV21USGS assigns a relatively larger fraction of vegetation over the Central Valley to broadleaf trees, which are biggest contributors of isoprene emissions (Fig. 3).

The differences in the spatial distributions of biogenic isoprene and monoterpene emissions due to various vegetation distributions is also illustrated by the average diurnal biogenic isoprene emission rates at the four observation sites shown in Figures 8 and 9. For example, the Mv21V3 simulation produces the largest biogenic isoprene and monoterpene emissions at three of the sites. At the T1 site over the forested foothills of the Sierra Nevada, the Mv21USGS and Mv21V3 simulations produce much larger biogenic isoprene emissions than Mv21V1 and Mv21V2. Even though forest is the dominant vegetation type along the foothills of the Sierra Nevada in all four vegetation datasets (Fig. 2), their different forest classifications and coverage result in biogenic isoprene emission rates that differ by as much as a factor of 8 at the T1 site. Similar to isoprene emissions, the Mv21USGS simulation produces the largest monoterpene emissions at the T1 site. However, the differences in monoterpene emissions among the four vegetation dataset experiments are smaller overall than that for biogenic isoprene emissions. Different vegetation distributions for a typical urban area can also lead to differences in biogenic isoprene and monoterpene emissions. For example at the urban

Geosci. Model Dev. Discuss., doi:10.5194/gmd-2015-266, 2016
Manuscript under review for journal Geosci. Model Dev.
Published: 19 January 2016

T0 and Pasadena sites, biogenic isoprene and monoterpene emission rates are almost 0 in the Mv21USGS and Mv21V1 experiments, while the rates were significant larger in the Mv21V3 experiment. This could have profound implications on local oxidant chemistry influencing urban air quality.

4.2.2 Isoprene+MVK+MACR and monoterpene mixing ratios

As expected, the differences in biogenic isoprene and monoterpene emissions among the four different vegetation distribution experiments lead to large differences in the simulated surface isoprene+MVK+MACR and monoterpene mixing ratios (Figs. 10a,b and 11a,b). Although all the four experiments simulate highest biogenic isoprene+MVK+MACR and monoterpene mixing ratios along the forested foothills of Sierra Nevada, the Mv21V1 and Mv21V3 experiments have the lowest isoprene+MVK+MACR and monoterpene mixing ratios, respectively, corresponding to their lowest biogenic emission rates. Over the Central Valley, Mv21USGS and Mv21V2 experiments produce significantly higher isoprene+MVK+MACR mixing ratios than the other two experiments, while Mv21V3 simulates the lowest monoterpene mixing ratios among all the experiments.

At the T1 site located in the forested foothills of Sierra Nevada, the Mv21V1 simulation produces the lowest isoprene+MVK+MACR mixing ratios (Fig. 12), significantly underestimating the peak concentrations during the day. In contrast, the Mv21USGS and Mv21V3 simulations reasonably capture the observed isoprene+MVK+MACR mixing ratios during the daytime. All four experiments underestimate the isoprene+MVK+MACR mixing ratios by about a factor of 2 during the night. This may indicate that the transported isoprene+MVK+MACR from the

Geosci. Model Dev. Discuss., doi:10.5194/gmd-2015-266, 2016
Manuscript under review for journal Geosci. Model Dev.
Published: 19 January 2016

surrounding areas of T1 was too low. The negative biases of simulated isoprene+MVK+MACR mixing ratios over the areas surrounding T1 can be reflected by Figure 14 that shows all the four experiments significantly underestimate the observed isoprene+MVK+MACR mixing ratios below 1 km in the northeast area around the T1 site (Fig. 10a). Figure 14 also shows that Mv21USGS and MV21V3 simulate larger isoprene+MVK+MACR mixing ratios averaged over the northeast region of northern California than Mv21V1 and Mv21V2. All four experiments produce similar surface monoterpene mixing ratios, which are smaller than that from the Mv20Noah and Mv20CLM with MEGAN v20 and are closer to the observed values particularly during the night. This is consistent with their much lower biogenic monoterpene emissions during the night (Fig. 9). The four experiments with MEGAN v21 simulate higher daytime monoterpene mixing ratios averaged along the flight tracks below 1 km than the two experiments with MEGAN v20. The simulated mixing ratios are still much lower than the aircraft observations, although the simulated surface mixing ratios are higher than the observations at the T1 site (Fig. 13). However, the aircraft measured monoterpene mixing ratios may also be higher than the true values due to the LOD of instruments (0.1-0.3 ppbv).

At the T0 site, an urban site, the vegetation coverage in both the Mv21USGS and Mv21V1 experiments is small so that the isoprene+MVK+MACR and monoterpene mixing ratios are significantly lower than observed during the daytime. The Mv21V2 and Mv21V3 experiments reasonably simulate isoprene+MVK+MACR mixing ratios during the daytime. Over the area surrounding the T0 site (i.e., the southwest area in Fig. 10a), it is interesting to note that the Mv21USGS and Mv21V2 simulations produced larger

Geosci. Model Dev. Discuss., doi:10.5194/gmd-2015-266, 2016
Manuscript under review for journal Geosci. Model Dev.
Published: 19 January 2016

576 isoprene+MVK+MACR mixing ratios than Mv21V1 and Mv21V3 and closer to the
577 observations (Fig. 14). This is mainly due to the relatively large isoprene+MVK+MACR
578 mixing ratios over the northwest corner of CARES sampling region (Fig. 10a) in the
579 Mv21USGS and Mv21V2 simulations, consistent with the distributions of biogenic
580 isoprene emissions over the region. The Mv21V2 and Mv21V3 simulations produced
581 higher monoterpene mixing ratios than Mv21USGS and Mv21V1, but are still smaller
582 than the observed values during the daytime not only for the T0 site but also for the
583 region surrounding T0 as shown in Figure 15.

584 At the Bakersfield site, only isoprene mixing ratios were reported. The
585 experiments often simulate significantly larger isoprene mixing ratios than the
586 observations, except for the Mv21V1 simulation that was always too small. The Mv21V3
587 simulation produced the highest isoprene mixing ratios among the experiments. This is
588 consistent with its biogenic isoprene emission rates (Fig. 8). In addition, the observed
589 surface isoprene mixing ratios show negligible diurnal variation in contrast to the
590 experiments that produced larger diurnal variations. The Mv21V3 simulation produced
591 peak isoprene mixing ratios during the daytime that were likely controlled by its large
592 daytime local biogenic isoprene emission rates (Fig. 8). The Mv21USGS and Mv21V2
593 simulations produced peak isoprene mixing ratios during the early evening, possibly the
594 result of chemistry and transport from regions with higher biogenic emissions. All four
595 experiments produce small diurnal variation of surface monoterpene mixing ratios. The
596 Mv21USGS and Mv21V3 simulations produce larger monoterpene mixing ratios than the
597 other two, consistent with their local emission rates (Fig. 9).

598 At the Pasadena site, the Mv21V3 simulation reproduces the observed diurnal

Geosci. Model Dev. Discuss., doi:10.5194/gmd-2015-266, 2016
Manuscript under review for journal Geosci. Model Dev.
Published: 19 January 2016

599 variation of isoprene+MVK+MACR mixing ratios reasonably well. This is consistent
600 with the area surrounding the Pasadena site, in which the Mv21V3 simulation produces
601 the largest mixing ratios of isoprene+MVK+MACR both at the surface (Fig. 10b) and
602 aloft (Fig. 14) in the vicinity of Los Angeles. The other three experiments simulated
603 significantly smaller mixing ratios of isoprene+MVK+MACR. Although the values from
604 the other three experiments are still smaller than the observations, they are much closer to
605 the aircraft measurements (within a factor of 2) than at the Pasadena site (Fig. 12).
606 Among the four vegetation sensitivity simulations, Mv21V3 produces higher surface
607 monoterpene mixing ratios than the other three experiments, consistent with their
608 emission rates (Fig. 9). All four vegetation sensitivity experiments produced much lower
609 monoterpene mixing ratios below 1 km (Fig. 15), compared to the aircraft measurements
610 over southern California that may overestimate the true values due to the LOD of
611 instruments (0.1-0.3 ppbv).

612 As discussed previously, all four experiments simulate significantly different
613 isoprene+MVK+MACR and monoterpene mixing ratios over the Central Valley (Figs.
614 10a,b and 11a,b). The Mv21USGS and Mv21V2 simulations produce much larger
615 isoprene+MVK+MACR mixing ratios (0.6 ppbV and 0.5 ppbV, respectively) over the
616 Central Valley than the observed values (~0.1 ppbV). The Mv21V1 and Mv21V3
617 simulations produce monoterpene mixing ratios much closer to observed values. This
618 may indicate that the fraction of broadleaf trees (the main emitter over the region) over
619 the Central Valley from the vegetation datasets USGS and VEG2 are overestimated or
620 the biogenic emission factors estimated for the broadleaf trees are overestimated for this
621 area. For monoterpenes, the Mv21V3 simulation was much smaller than observed, while

Geosci. Model Dev. Discuss., doi:10.5194/gmd-2015-266, 2016
Manuscript under review for journal Geosci. Model Dev.
Published: 19 January 2016

the mixing ratios from the other three experiments were more comparable. This suggests that the fraction of vegetation emitting monoterpenes is significantly underestimated over this area in the VEG3 dataset.

5. Summary and discussion

In this study, the latest version of MEGAN (v2.1) is coupled within the CLM4 land scheme as part of WRF-Chem. Specifically, MEGAN v2.1 is implemented into the CLM4 scheme so that a consistent vegetation map can be used for estimating biogenic VOC emissions as well as surface fluxes. This is unlike the older version of MEGAN (v2.0) in the public-released WRF-Chem that uses a standalone vegetation map that differs from what is used in land surface schemes. With this improved WRF-Chem modeling framework coupled with CLM4-MEGAN v2.1, the sensitivity of biogenic VOC emissions and hence the atmospheric VOC mixing ratios to vegetation distributions is investigated. The WRF-Chem simulations are also conducted with the two land surface schemes, Noah and CLM4, with the MEGAN v2.0 scheme for biogenic emissions in each case. The comparison between the Noah and CLM4 driven MEGAN v2.0 biogenic emissions not only serves for investigating the impact of different land surface schemes on the emissions but also provides a reference for all previous studies that used the Noah land surface scheme. Experiments are conducted for June 2010 over California, compared with the measurements from the CARES and CalNex campaigns. The main findings about the modeling sensitivity to the land surface schemes and vegetation distributions include:

- The WRF-Chem simulation with the CLM4 land surface scheme and the MEGAN

Geosci. Model Dev. Discuss., doi:10.5194/gmd-2015-266, 2016
Manuscript under review for journal Geosci. Model Dev.
Published: 19 January 2016

v2.0 module (Mv20CLM) produces similar biogenic isoprene and monoterpene emissions in terms of spatial patterns, magnitudes, and diurnal variations as the one with the Noah land surface scheme (Mv20Noah) in June over California. The similarity in the biogenic emissions between the experiments using two different land schemes is primarily because of using MEGAN v2.0 and the same vegetation map in the two experiments. The spatial patterns and magnitudes of surface isoprene+MVK+MACR and monoterpene mixing ratios are generally similar between the two experiments with the Noah and CLM4 land surface schemes, although there are significant differences at some specific locations due to their differences in the near surface meteorology such as surface net radiation and temperature. Compared with surface and aircraft measurements, both experiments generally underestimate the daytime mixing ratios of isoprene+MVK+MACR but overestimate the nighttime mixing ratios of monoterpenes.

- The experiments with the four vegetation datasets result in much larger differences in biogenic isoprene and monoterpene emissions than the ones with the two land surface schemes. The simulated total biogenic isoprene and monoterpene emissions over California can differ by a factor of 3 among the experiments and the difference can be even larger over specific locations. The comparison of mixing ratios of isoprene+MVK+MACR and monoterpenes with the observations indicates the simulation biases can be largely reduced with accurate vegetation distributions over some regions of California. For example, at an observation site at the forested foothills of Sierra Nevada, two experiments with the vegetation distributions from the USGS and VEG3 datasets capture the observed daytime surface mixing ratios of

Geosci. Model Dev. Discuss., doi:10.5194/gmd-2015-266, 2016
Manuscript under review for journal Geosci. Model Dev.
Published: 19 January 2016

isoprene+MVK+MACR well, with values that are much larger than the experiments with the other two vegetation datasets.

- Although vegetation distributions from some datasets do significantly improve the model performance in simulating BVOCs mixing ratios more than others, the optimal vegetation dataset cannot be determined, because the improvement by vegetation datasets has dependence on both the region and BVOC species of interest. For example, over the Central Valley, the experiments with the VEG1 and VEG3 vegetation datasets simulate isoprene+MVK+MACR mixing ratios that are much closer to observations than the USGS and VEG2 datasets, while the VEG3 dataset significantly underestimates the observed monoterpene mixing ratios. Large biases over some regions of California in all the experiments with current vegetation datasets imply that more effort is needed to improve land cover datasets and/or biogenic emission factors.

There are still some large biases existing over some regions of California regardless of the vegetation distributions. For example, all the experiments significantly underestimate the observed isoprene+MVK+MACR mixing ratios below an altitude of 1 km over the forest-covered Sierra Nevada. Over the Pasadena area, all the experiments simulate significantly smaller monoterpene mixing ratios than observed. The biases in BVOCs identified in this study may be partly due to inaccurate vegetation distributions in all the vegetation distribution datasets. The biases can also result from the uncertainties in BVOCs emission factors for the individual types of vegetation commonly found in California. The constraints on BVOCs emission factors applied in models are limited due to sparse measurements of BVOCs emission fluxes. The MEGAN scheme in WRF-Chem

Geosci. Model Dev. Discuss., doi:10.5194/gmd-2015-266, 2016
Manuscript under review for journal Geosci. Model Dev.
Published: 19 January 2016

691 uses the global averaged emission factors for BVOCs emissions for each PFT. Over
692 California, the broadleaf temperate trees are primarily oaks that have relatively higher
693 BVOCs emission factors compared to the global mean values for temperate broadleaf
694 trees. In addition, the needleleaf trees are pines that have relatively larger monoterpene
695 emission factors compared to global mean values. These biases in emission factors may
696 partly explain why all the experiments generally underestimate mixing ratios of
697 isoprene+MVK+MACR and monoterpenes over the regions with large amounts of trees.
698 The MEGAN scheme using the location-specified emission factor maps that accounts for
699 species composition of trees may provide a better estimate on regional scales.

700 This study demonstrates large difference between the experiments with the two
701 versions of MEGAN (v20 versus v21), and that MEGAN v21 results in a better
702 comparison with the observations over some parts of the study domain. However, this
703 difference should not be fully attributed to the improvement of MEGAN between the two
704 versions, because the two versions also use different vegetation distributions. The results
705 highlight the importance of sub-grid vegetation distributions in simulating biogenic
706 emissions even at a relatively high horizontal grid spacing (e.g., 4 km in this study). The
707 biogenic emissions can be significantly different even though the dominant vegetation
708 within a model grid box is similar. The comparison of the simulations and the
709 observations at the surface sites and along the aircraft tracks reflects the large spatial
710 variability of biogenic emissions and BVOCs mixing ratios over California. It is
711 challenging for model to capture such a spatial heterogeneity of BVOCs if the vegetation
712 distributions are not appropriately represented in the simulation. The relatively large
713 LOD of instruments on the aircrafts for monoterpenes compared to the true

Geosci. Model Dev. Discuss., doi:10.5194/gmd-2015-266, 2016
Manuscript under review for journal Geosci. Model Dev.
Published: 19 January 2016

concentrations also make the evaluation of simulated monoterpenes difficult. Over a region with relatively low monoterpene concentrations, an instrument with lower LOD is needed. Finally, it is also noteworthy that factors other than biogenic emissions can influence the simulated BVOCs mixing ratios over California, such as anthropogenic emissions and the oxidation mechanism of BVOCs used in simulations. Therefore, additional direct measurements of biogenic emission fluxes are needed for a better evaluation of simulated BVOCs fluxes.

Code availability

The WRF-Chem version 3.5.1 release can be obtained at http://www2.mmm.ucar.edu/wrf/users/download/get_source.html. Code modifications for implementing MEGANv2.1 into CLM are available upon request by contacting the corresponding author and will be released to public WRF-Chem version.

Acknowledgements

This was work was supported by the U.S. Department of Energy, Office of Science, Office of Biological and Environmental Research's Atmospheric Systems Research (ASR) Program and Atmospheric Radiation Measurement (ARM) Climate Research Facility. A portion of this research was supported by the US NOAA's Atmospheric Composition and Climate Program (NA11OAR4310160). The simulations required for this work were performed on the National Energy Research Scientific Computing Center, supported by the Office of Science of the U.S. Department of Energy. We acknowledge Dr. Tom Jobson and Dr. Bentram Knighton for their measurements during the CARES

Geosci. Model Dev. Discuss., doi:10.5194/gmd-2015-266, 2016
Manuscript under review for journal Geosci. Model Dev.
Published: 19 January 2016

737 campaign. The Pacific Northwest National Laboratory is operated for DOE by Battelle
738 Memorial Institute under contract DE-AC05-76RL01830. NCAR is operated by the
739 University Corporation of Atmospheric Research under sponsorship of the National
740 Science Foundation.

741

742
743

Geosci. Model Dev. Discuss., doi:10.5194/gmd-2015-266, 2016
Manuscript under review for journal Geosci. Model Dev.
Published: 19 January 2016

Reference

Andreae, M. and P. J. Crutzen: Atmospheric Aerosols : Biogeochemical Sources and Role in Atmospheric Chemistry. Science, 276, 5315, 1052-1058, doi:10.1126/science.276.5315.1052, 1997.

Arneth, A., S. P. Harrison, S. Zaehle, K. Tsigaridis, S. Menon, P. J. Bartlein, J. Feichter, A. Korhola, M. Kulmala, D. O'Donnell, G. Schurgers, S. Sorvari, and T. Vesala: Terrestrial biogeochemical feedbacks in the climate system, Nature Geoscience, 3, 525-532, 2000.

Arneth, A., Niinemets, Ü., Pressley, S., Bäck, J., Hari, P., Karl, T., Noe, S., Prentice, I. C., Serça, D., Hickler, T., Wolf, A., and Smith, B.: Process ‐ based estimates of terrestrial ecosystem isoprene emissions: Incorporating the effects of a direct CO2 ‐ isoprene interaction, Atmos. Chem. Phys., 7, 31–53, 2007.

Barlage, M., F. Chen, M. Tewari, K. Ikeda, D. Gochis, J. Dudhia, R. Rasmussen, B. Livneh, M. Ek, and K. Mitchell: Noah land surface model modifications to improve snowpack prediction in the Colorado Rocky Mountains, J. Geophys. Res., 115, D22101, doi:10.1029/2009JD013470, 2010.

Bonan, G. B.: A land surface model (LSM ver. 1.0) for ecological, hydrological, and atmospheric studies: Technical description and user's guide. NCAR Tech. Note 4171STR, 150 pp, 1996.

Bonan, G. B., K. W. Oleson, M. Vertenstein, S. Levis, X. Zeng, Y. Dai, R. E. Dickinson, and Z.-L. Yang: The Land Surface Climatology of the Community Land Model Coupled to the NCAR Community Climate Model. J. Climate, 15, 3123–3149, doi: http://dx.doi.org/10.1175/1520-0442(2002)015<3123:TLSCOT>2.0.CO;2, 2002.

Geosci. Model Dev. Discuss., doi:10.5194/gmd-2015-266, 2016
Manuscript under review for journal Geosci. Model Dev.
Published: 19 January 2016

767 Carter,W. P. L.: Documentation of the SAPRC-99 Chemical Mechanism for VOC
768 Reactivity Assessment, Draft report to the California Air Resources Board, Contracts
769 92–329 and 95–308, 8 May, available at: http://www.cert.ucr.edu/~carter/pubs/ (last
770 access:1 December 2015), 2000a.
771 Carter,W. P. L.: Implementation of the SAPRC-99 Chemical Mechanism into the
772 Models-3 Framework, Report to the United States Environmental Protection Agency,
773 29 January, available at: http://www.cert.ucr.edu/~carter/pubs/ (last access: 1
774 December 2015), 2000b.
775 Chameides, W. L., F. Fehsenfeld, M. O. Rodgers, C. Cardelino, J. Martinez, D. Parrish,
776 W. Lonneman, D. R. Lawson, R. A. Rasmussen, P. Zimmerman, J. Greenberg, P.
777 Mlddleton, T. Wang: Ozone precursor relationships in the ambient atmosphere, J.
778 Geophys. Res., 97(D5), 6037–6055, doi:10.1029/91JD03014, 1992.
779 Claeys, M., B. Graham, G. Vas, W. Wang, R. Vermeylen, V. Pashynska, J. Cafmeyer, P.
780 Guyon, M. O. Andreae, P. Artaxo, W. Maenhaut: Formation of Secondary Organic
781 Aerosols Through Photooxidation of Isoprene, Vol. 303 no. 5661 pp. 1173-1176, doi:
782 10.1126/science.1092805, 2004.
783 Cox, P., Delao, A., Komorniczak, A., andWeller, R.: The California almanac of
784 emissions and air quality 2009 edition,
785 http://www.arb.ca.gov/aqd/almanac/almanac09/almanac2009all.pdf, 2009.
786 Dickinson R. E.: Land Surface Processes and Climate Surface Albedos and Energy-
787 Balance. Adv Geophys 25:305-353. doi: 10.1016/S0065-2687(08)60176-4, 1983.

Geosci. Model Dev. Discuss., doi:10.5194/gmd-2015-266, 2016
Manuscript under review for journal Geosci. Model Dev.
Published: 19 January 2016

788 Duhl, T. R., Guenther, A., and Helmig, D.: Estimating urban vegetation cover fraction
789 using Google Earth®images, J. Land Use Sci., 7, 311–329,
790 doi:10.1080/1747423X.2011.587207, 2012.
791 Fast, J. D, Gustafson Jr., W. I., Easter, R. C., Zaveri, R. A., Barnard, J. C., Chapman, E.
792 G., and. Grell, G. A.: Evolution of ozone, particulates, and aerosol direct forcing in an
793 urban area using a new fully-coupled meteorology, chemistry, and aerosol model, J.
794 Geophys. Res., 111, D21305, doi:10.1029/2005JD006721, 2006.
795 Fast, J. D., Allan, J., Bahreini, R., Craven, J., Emmons, L., Ferrare, R., Hayes, P. L.,
796 Hodzic, A., Holloway, J., Hostetler, C., Jimenez, J. L., Jonsson, H., Liu, S., Liu, Y.,
797 Metcalf, A., Middlebrook, A., Nowak, J., Pekour, M., Perring, A., Russell, L.,
798 Sedlacek, A., Seinfeld, J., Setyan, A., Shilling, J., Shrivastava, M., Springston, S.,
799 Song, C., Subramanian, R., Taylor, J. W., Vinoj, V., Yang, Q., Zaveri, R. A., and
800 Zhang, Q.: Modeling regional aerosol and aerosol precursor variability over
801 California and its sensitivity to emissions and long-range transport during the 2010
802 CalNex and CARES campaigns, Atmos. Chem. Phys., 14, 10013-10060,
803 doi:10.5194/acp-14-10013-2014, 2014.
804 Fehsenfeld, F., Calvert, J., Fall, R., Goldan, P., Guenther, A.B., Hewitt, C.N., Lamb, B.,
805 Liu, S., Trainer, M., Westberg, H. and Zimmerman, P.: Emissions of volatile organic
806 compounds from vegetation and the implications for atmospheric chemistry. Global
807 Biogeochemical Cycles, 6: doi: 10.1029/92GB02125. issn: 0886-6236, 1992.
808 Gao, Y., X. Liu, C. Zhao, and M. Zhang: Emission controls versus meteorological
809 conditions in determining aerosol concentrations in Beijing during the 2008 Olympic
810 Games, Atmos. Chem. Phys., 11, 12437-12451, 2011.

Geosci. Model Dev. Discuss., doi:10.5194/gmd-2015-266, 2016
Manuscript under review for journal Geosci. Model Dev.
Published: 19 January 2016

811 Gao, Y., C. Zhao, X. Liu, M. Zhang, and L. R. Leung: Regional modeling of aerosol and
812 its radiative forcing over East Asia using WRF-Chem, Atmos. Environ., 92, 250-266,
813 2014.
814 Gentner, D. R., Isaacman, G., Worton, D. R., Chan, A. W. H., Dallmann, T. R., Davis, L.,
815 Liu, S., Day, D. A., Russell, L. M., Wilson, K. R., Weber, R., Guha, A., Harley, R.
816 A., and Goldstein, A. H.: Elucidating secondary organic aerosol from diesel and
817 gasoline vehicles through detailed characterization of organic carbon emissions, P.
818 Natl. Acad. Sci. USA, 109, 18318–18323, doi:10.1073/pnas.1212272109, 2012.
819 Greenfield, E.J., D.J. Nowak, and J.T. Walton: Assessment of 2001 NLCD percent tree
820 and impervious cover estimates, Photogrammetric Engineering & Remote Sensing ,
821 75(11): 1279–1286, 2009.
822 Grell, G. A., Peckham, S. E., Schmitz, R., and McKeen, S. A., Frost, G., Skamarock, W.
823 C., and Eder, B.: Fully coupled “online” chemistry within the WRF model, Atmos.
824 Environ., 39, 6957–6976, 2005.
825 Guenther, A. B., P. R. Zimmerman, P. C. Harley, R. K. Monson, and R. Fall: Isoprene
826 and monoterpene emission rate variability: model evaluations and sensitivity
827 analyses. Journal of Geophysical Research, vol. 98, no. 7, pp. 12–617, 1993.
828 Guenther, A. B., Hewitt, C. N., Erickson, D., Fall, R., Geron, C., Graedel, T., Harley, P.,
829 Klinger, L., Lerdau, M., McKay, W. A., Pierce, T., Scholes, B., Steinbrecher, R.,
830 Tallamraju, R., Taylor, J., and Zimmerman, P.: A global model of natural volatile
831 organic compound emissions, J. Geophys. Res.-Atmos., 100, 8873–8892, 1995.
832 Guenther, A. B., W. Baugh, K. Davis, Gary Hampton, P. Harley, L. Klinger, L. Vierling,
833 P. Zimmerman, E. Allwine, S. Dilts, B. Lamb, H. Westberg, D. Baldocchi, C. Geron,

Geosci. Model Dev. Discuss., doi:10.5194/gmd-2015-266, 2016
Manuscript under review for journal Geosci. Model Dev.
Published: 19 January 2016

834 T. Pierce: Isoprene fluxes measured by enclosure, relaxed eddy accumulation, surface
835 layer gradient, mixed layer gradient, and mixed layer mass balance techniques.
836 Journal of Geophysical Research D, vol. 101, no. 13, pp. 18555–18567, 1996.
837 Guenther, A., T. Karl, P. Harley, C. Wiedinmyer, P. I. Palmer, and C. Geron: Estimates
838 of global terrestrial isoprene emissions using MEGAN (Model of Emissions of Gases
839 and Aerosols from Nature). Atmospheric Chemistry and Physics, vol. 6, no. 11, pp.
840 3181–3210, 2006.
841 Guenther, A. B., Jiang, X., Heald, C. L., Sakulyanontvittaya, T., Duhl, T., Emmons, L.
842 K., and Wang, X.: The Model of Emissions of Gases and Aerosols from Nature
843 version 2.1 (MEGAN2.1): an extended and updated framework for modeling biogenic
844 emissions, Geosci. Model Dev., 5, 1471-1492, doi:10.5194/gmd-5-1471-2012, 2012.
845 Guenther, A. B.: Biological and chemical diversity of biogenic volatile organic emissions
846 into the atmosphere, ISRN Atmospheric Sciences, 2013, 786290, 1-27, 2013.
847 Hong, Song-You, Yign Noh, Jimy Dudhia: A new vertical diffusion package with an
848 explicit treatment of entrainment processes. Mon. Wea. Rev., 134, 2318–2341, 2006.
849 Huang, M., Carmichael, G. R., Spak, S. N., Adhikary, B., Kulkarni, S., Cheng, Y., Wei,
850 C., Tang, Y., D'Allura, A., Wennberg, P. O., Huey, G. L., Dibb, J. E., Jimenez, J. L.,
851 Cubison, M. J., Weinheimer, A. J., Kaduwela, A., Cai, C., Wong, M., Bradley Pierce,
852 R., Al-Saadi, J. A., Streets, D. G., and Zhang, Q.: Multi-scale modeling study of the
853 source contributions to near-surface ozone and sulfur oxides levels over California
854 during the ARCTAS-CARB period, Atmos. Chem. Phys., 11, 3173-3194,
855 doi:10.5194/acp-11-3173-2011, 2011.

Geosci. Model Dev. Discuss., doi:10.5194/gmd-2015-266, 2016
Manuscript under review for journal Geosci. Model Dev.
Published: 19 January 2016

856 Hijmas, R. J., S. E. Cameron, J. L. Parra, P. G. Jones, and A. Jarvis: Very high resolution
857 interpolated climate surfaces for global land areas. Int. J. Climatol. 25: 1965–1978
858 (2005), DOI: 10.1002/joc.1276, 2005.
859 Iacono, M. J., J. S. Delamere, E. J. Mlawer, M. W. Shephard, S. A. Clough, and W. D.
860 Collins: Radiative forcing by long–lived greenhouse gases: Calculations with the
861 AER radiative transfer models. J. Geophys. Res., 113, D13103, 2008.
862 Jin, J., and N. L. Miller (2007), Analysis of the impact of snow on dailyweather
863 variability in mountainous regions using MM5, J. Hydrometeorol.,8, 245 –258,
864 doi:10.1175/JHM565.1.
865 Jin, J., and L. Wen: Evaluation of snowmelt simulation in the Weather Research and
866 Forecasting model, J. Geophys. Res., 117, D10110, doi:10.1029/2011JD016980,
867 2012.
868 Kain, John S.: The Kain–Fritsch convective parameterization: An update. J. Appl.
869 Meteor., 43, 170–181, 2004.
870 Ke Y, LYR Leung, M Huang, AM Coleman, H Li, and MS Wigmosta: Development of
871 High Resolution Land Surface Parameters for the Community Land Model.
872 Geoscientific Model Development 5(6):1341-1362. doi:10.5194/gmd-5-1341-2012,
873 2012.
874 Knote, C., Hodzic, A., Jimenez, J. L., Volkamer, R., Orlando, J. J., Baidar, S., Brioude,
875 J., Fast, J., Gentner, D. R., Goldstein, A. H., Hayes, P. L., Knighton, W. B., Oetjen,
876 H., Setyan, A., Stark, H., Thalman, R., Tyndall, G., Washenfelder, R., Waxman, E.,
877 and Zhang, Q.: Simulation of semi-explicit mechanisms of SOA formation from

878 glyoxal in aerosol in a 3-D model, Atmos. Chem. Phys., 14, 6213-6239,
879 doi:10.5194/acp-14-6213-2014, 2014.
880 Lamb, B., A. Guenther, D. Gay, H. Westberg: A national inventory of biogenic
881 hydrocarbon emissions. Atmos. Environ., 21, 8, 1695-1705, doi:10.1016/0004-
882 6981(87)90108-9, 1987.
883 Lawrence, P.J. and T.N. Chase: Climate Impacts. Our earth's changing land: an
884 encyclopedia of land-use and land-cover change, H. Geist, Greenwood Press,
885 Westport, 115-124, 2006.
886 Lawrence, P. J. and T. N. Chase: Representing a new MODIS consistent land surface in
887 the Community Land Model (CLM 3.0). J. Geophys. Res.-Biogeosci.: Vol. 112,
888 2007.
889 Lawrence, D.M., K.W. Oleson, M.G. Flanner, P.E. Thornton, S.C. Swenson, P.J.
890 Lawrence, X. Zeng, Z.-L. Yang, S. Levis, K. Sakaguchi, G.B. Bonan, and A.G.
891 Slater: Parameterization improvements and functional and structural advances in
892 version 4 of the Community Land Model. J. Adv. Model. Earth Sys., 3, DOI:
893 10.1029/2011MS000045, 2011.
894 Lemone, M. A., F. Chen, M. Tewari, J. Dudhia, B. Geerts, Q. Miao, R. L. Coulter, and R.
895 L. Grossman (2010a), Simulating the IHOP_2002 Fair-Weather CBL with the WRF-
896 ARW-Noah modeling system. Part I: Surface fluxes and CBL structure and evolution
897 along the eastern track, Mon. Weather Rev., 138(3), 722–744,
898 doi:10.1175/2009mwr3003.1.
899 Lemone, M. A., F. Chen, M. Tewari, J. Dudhia, B. Geerts, Q. Mia, R. L. Coulter, and R.
900 L. Grossman (2010b), Simulating the IHOP_2002 Fair-Weather CBL with the WRF-

Geosci. Model Dev. Discuss., doi:10.5194/gmd-2015-266, 2016
Manuscript under review for journal Geosci. Model Dev.
Published: 19 January 2016

ARW Noah modeling system. Part II: Structures from a few kilometers to 100 km across, Mon. Weather Rev., 138(3), 745–764, doi:10.1175/2009mwr3004.1.

Lindinger, W., Hansel, A., and Jordan, A.: On-line monitoring of volatile organic compounds at pptv levels by means of protontransfer-reaction mass spectrometry (PTR-MS) – medical applications, food control and environmental research, Int. J. Mass Spectrom., 173, 191–241, 1998.

McKeen, S. A., G. Wotawa, D. D. Parrish, J. S. Holloway, M. P. Buhr, G. Hubler, F. C. Fehsenfeld, and J. F. Meagher: Ozone production from Canadian wildfires during June and July of 1995, J. Geophys. Res., 107(D14), 4192, doi:10.1029/2001JD000697, 2002.

Morrison, H., G. Thompson, V. Tatarskii: Impact of Cloud Microphysics on the Development of Trailing Stratiform Precipitation in a Simulated Squall Line: Comparison of One– and Two–Moment Schemes. Mon. Wea. Rev., 137, 991–1007, 2009.

Müller J.-F.: Geographical distribution and seasonal variation of surface emissions and deposition veloci- ties of atmospheric trace gases. J. Geophys. Res. 97(D4): 3787–3804, 1992.

Niinemets, Ü., J. D. Tenhunen, P. C. Harley, and R. Steinbrecher: A model of isoprene emission based on energetic requirements for isoprene synthesis and leaf photosynthetic properties for Liquidambar and Quercus, Plant Cell Environ., 22, 1319–1335, 1999.

Geosci. Model Dev. Discuss., doi:10.5194/gmd-2015-266, 2016
Manuscript under review for journal Geosci. Model Dev.
Published: 19 January 2016

922 Niinemets, Ü., G. Seufert, R. Steinbrecher, and J. D. Tenhunen: A model coupling foliar
923 monoterpene emissions to leaf photosynthetic characteristics in Mediterranean
924 evergreen Quercus species, New Phytol., 153, 257–275, 2002.
925 Oleson, K. W., Lawrence, D. M., Bonan, G. B., Flanner, M. G., Kluzek, E., Lawrence, P.
926 J., Levis, S., Swenson, S. C., Thornton, P. E., Dai, A., Decker, M., Dickinson, R.,
927 Feddema, J., Heald, C. L., Hoffman, F., Lamarque, J.-F., Mahowald, N., Niu, G.-Y.,
928 Qian, T., Randerson, J., Running, S., Sakaguchi, K., Slater, A., Sto¨ckli, R., Wang,
929 A., Yang, Z.-L., Zeng, X., and Zeng, X.: Tech- nical Description of version 4.0 of the
930 Community Land Model (CLM), Tech. Rep. NCAR/TN-478 + STR, National Center
931 for Atmospheric Research, 2010.
932 Oliver Wild, Xin Zhu, Michael J. Prather: Fast-J: Accurate Simulation of In- and Below-
933 Cloud Photolysis in Tropospheric Chemical Models, J. Atmos. Chem., Volume 37,
934 Issue 3, pp 245-282, 2000.
935 Paulson, C. A.: The mathematical representation of wind speed and temperature profiles
936 in the unstable atmospheric surface layer. J. Appl. Meteor., 9, 857–861, 1970.
937 Pfister, G. G., Parrish, D. D.,Worden, H., Emmons, L. K., Edwards, D. P., Wiedinmyer,
938 C., Diskin, G. S., Huey, G., Oltmans, S. J., Thouret, V., Weinheimer, A., and
939 Wisthaler, A.: Characterizing summertime chemical boundary conditions for air
940 masses entering the US West Coast, Atmos. Chem. Phys., 11, 1769–1790,
941 doi:10.5194/acp-11-1769-2011, 2011.
942 Pierce, T., C. Geron, L. Bender, R. Dennis, G. Tonnesen, and A. Guenther: Influence of
943 increased isoprene emissions on regional ozone modeling, J. Geophys. Res.,
944 103(D19), 25611–25629, doi:10.1029/98JD01804, 1998.

945 Poisson, N., M. Kanakidou, P. J. Crutzen: Impact of Non-Methane Hydrocarbons on
946 Tropospheric Chemistry and the Oxidizing Power of the Global Troposphere: 3-
947 Dimensional Modelling Results, J. Atmos. Chem., 36, 157-230, 2000.
948 Rasmussen, R. A.: What do the hydrocarbons from trees contribute to air pollution? J. Air
949 Poll. Con. Asso., 22, 7, 537-543, 1972.
950 Ryerson, T. B., Andrews, A. E., Angevine, W. M., Bates, T. S., Brock, C. A., Cairns, B.,
951 Cohen, R. C., Cooper, O. R., de Gouw, J. A., Fehsenfeld, R. C., Ferrare, R. A.,
952 Fischer, M. L., Flagan, R. C., Goldstein, A. H., Hair, J. W., Hardesty, R. M.,
953 Hostetler, C. A., Jimenez, J. L., Langford, A. O., McCauley, E., McKeen, S. A.,
954 Molina, L. T., Nenes, A., Oltmans, S. J., Parrish, D. D., Pederson, J. R., Pierce, R. B.,
955 Prather, K., Quinn, P. K., Seinfeld, J. H., Senff, C. J., Sorooshian, A., Stutz, J.,
956 Surratt, J. D., Trainer, M., Volkamer, R., Williams, E. J., and Wofsy, S. C.: The 2010
957 California Research at the Nexus of Air Quality and Climate Change (CalNex) field
958 study, J. Geophys. Res., 118, 5830-5866, doi:10.1002/jgrd.50331, 2013.
959 Sakulyanontvittaya, T., Duhl, T., Wiedinmyer, C., Helmig, D., Mat- sunaga, S.,
960 Potosnak, M., Milford, J., and Guenther, A.: Monoter- pene and sesquiterpene
961 emission estimates for the United States, Environ. Sci. Technol., 42, 1623–1629,
962 2008.
963 Sanderson, M.G., Jones, C.D., Collins, W.J., Johnson, C.E. and Derwent, R.G.: Effect of
964 Climate Change on Isoprene Emissions and Surface Ozone Levels. Geophysical
965 Research Letters 30: doi: 10.1029/2003GL017642. issn: 0094-8276, 2003.

Geosci. Model Dev. Discuss., doi:10.5194/gmd-2015-266, 2016
Manuscript under review for journal Geosci. Model Dev.
Published: 19 January 2016

966 Schurgers, G., A. Arneth, R. Holzinger, and A. Goldstein: Processbased modelling of
967 biogenic monoterpene emissions combining production and release from storage,
968 Atmos. Chem. Phys., 9, 3409–3423, 2009.
969 Shilling, J. E., R. A. Zaveri, J. D. Fast, L. I. Kleinman, M. L. Alexander, M. R.
970 Canagaratna, E. Fortner, J. M. Hubbe, J. T. Jayne, A. Sedlacek, A. Setyan, S.
971 Springston, D. R. Worsnop, and Q. Zhang: Enhanced SOA formation from mixed
972 anthropogenic and biogenic emissions during the CARES campaign. Atmospheric
973 Chemistry and Physics, 13(4):2091-2113, doi:10.5194/acp-13-2091-2013, 2013.
974 Shrivastava MKB, JD Fast, RC Easter, Jr, WI Gustafson, Jr, RA Zaveri, JL Jimenez, P
975 Saide, and A Hodzic: Modeling Organic Aerosols in a Megacity: Comparison of
976 Simple and Complex Representations of the Volatility Basis Set Approach.
977 Atmospheric Chemistry and Physics 11(13):6639-6662. doi:10.5194/acp-11-6639-
978 2011.
979 Shrivastava MKB, A Zelenyuk, D Imre, RC Easter, Jr, J Beranek, RA Zaveri, and JD
980 Fast: Implications of Low Volatility SOA and Gas-Phase Fragmentation Reactions on
981 SOA Loadings and their Spatial and Temporal Evolution in the Atmosphere. Journal
982 of Geophysical Research. D. (Atmospheres), 118(8), 3328-3342,
983 doi:10.1002/jgrd.50160, 2013.
984 Stauffer, D. R. and Seaman, N. L.: Use of four-dimensional data assimilation in a limited-
985 area mesoscale model, Part I: Experiments with synoptic-scale data, Mon. Weather
986 Rev., 118, 1250–1277, 1990.

Geosci. Model Dev. Discuss., doi:10.5194/gmd-2015-266, 2016
Manuscript under review for journal Geosci. Model Dev.
Published: 19 January 2016

987 Still, C. J., J. A. Berry, G. J. Collatz, and R. S. DeFries, Global distribution of C3 and C4
988 vegetation: Carbon cycle implications, Global Biogeochem. Cycles, 17(1), 1006,
989 doi:10.1029/2001GB001807, 2003.
990 Went, F. W.: blue hazes in the atmosphere, Nature, Vol. 187, 4738, 641-643, 1960.
991 Wild, O., X. Zhu, and Prather, M. J.: Fast-J: Accurate simulation of in- and below-cloud
992 photolysis in tropospheric chemical models. Journal of Atmospheric Chemistry,
993 37(3), 245 - 282. doi: 10.1023/A:1006415919030, 2000.
994 Willmott, C. J. and K. Matsuura: Terrestrial Air Temperature and Precipitation: Monthly
995 and Annual Time Series (1950 - 1999), 2011
996 (http://climate.geog.udel.edu/~climate/html_pages/README.ghcn_ts2.html).
997 Zaveri, R. A., Shaw, W. J., Cziczo, D. J., Schmid, B., Ferrare, R. A., Alexander, M. L.,
998 Alexandrov, M., Alvarez, R. J., Arnott, W. P., Atkinson, D. B., Baidar, S., Banta, R.
999 M., Barnard, J. C., Beranek, J., Berg, L. K., Brechtel, F., Brewer, W. A., Cahill, J. F.,
1000 Cairns, B., Cappa, C. D., Chand, D., China, S., Comstock, J. M., Dubey, M. K.,
1001 Easter, R. C., Erickson, M. H., Fast, J. D., Floerchinger, C., Flowers, B. A., Fortner,
1002 E., Gaffney, J. S., Gilles, M. K., Gorkowski, K., Gustafson, W. I., Gyawali, M., Hair,
1003 J., Hardesty, R. M., Harworth, J. W., Herndon, S., Hiranuma, N., Hostetler, C.,
1004 Hubbe, J. M., Jayne, J. T., Jeong, H., Jobson, B. T., Kassianov, E. I., Kleinman, L. I.,
1005 Kluzek, C., Knighton, B., Kolesar, K. R., Kuang, C., Kubátová, A., Langford, A. O.,
1006 Laskin, A., Laulainen, N., Marchbanks, R. D., Mazzoleni, C., Mei, F., Moffet, R. C.,
1007 Nelson, D., Obland, M. D., Oetjen, H., Onasch, T. B., Ortega, I., Ottaviani, M.,
1008 Pekour, M., Prather, K. A., Radney, J. G., Rogers, R. R., Sandberg, S. P., Sedlacek,
1009 A., Senff, C. J., Senum, G., Setyan, A., Shilling, J. E., Shrivastava, M., Song, C.,

1010 Springston, S. R., Subramanian, R., Suski, K., Tomlinson, J., Volkamer, R., Wallace,
1011 H. W., Wang, J., Weickmann, A. M., Worsnop, D. R., Yu, X.-Y., Zelenyuk, A., and
1012 Zhang, Q.: Overview of the 2010 Carbonaceous Aerosols and Radiative Effects Study
1013 (CARES), Atmos. Chem. Phys., 12, 7647-7687, doi:10.5194/acp-12-7647-2012,
1014 2012.
1015 Zeng, X., M. Shaikh, Y. Dai, R. E. Dickinson, and R. Myneni (2002), Cou-pling of the
1016 common land model to the NCAR community climate model,J. Clim., 15, 1832–
1017 1854, doi:10.1175/1520-0442(2002)015<1832:COTCLM>2.0.CO;2.
1018 Zhao, C., Hu, Z., Qian, Y., Ruby Leung, L., Huang, J., Huang, M., Jin, J., Flanner, M. G.,
1019 Zhang, R., Wang, H., Yan, H., Lu, Z., and Streets, D. G.: Simulating black carbon
1020 and dust and their radiative forcing in seasonal snow: a case study over North China
1021 with field campaign measurements, Atmos. Chem. Phys., 14, 11475-11491,
1022 doi:10.5194/acp-14-11475-2014, 2014.
1023 Zimmerman, P. R., R. B. Chatfield, J. Fishman, P. J. Crutzen, and P. L. Hanst, Estimates
1024 the production of CO and H2 from the oxidation of hydrocarbon emissions from
1025 vegetation, Geophys. Res. Lett., 5, 679-682, 1978.
1026 Zimmerman, P.: Testing of hydrocarbon emissions from vegetation, leaf litter and aquatic
1027 surfaces and development of a method for compiling biogenic emission inventories,
1028 Tech. Rep. EPA-450-4-70-004, U.S. Environmental Protection Agency, Research
1029 Triangle Park, California, USA, 1979.
1030
1031

Geosci. Model Dev. Discuss., doi:10.5194/gmd-2015-266, 2016
Manuscript under review for journal Geosci. Model Dev.
Published: 19 January 2016

Geoscientific Model Development Discussions

Table 1 Average percentage of PFT's over the simulation domain

PFT # and description		USGS	VEG1	VEG2	VEG3
0	**Bare soil**	26.0	7.6	38.1	41.6
1	**Needleleaf evergreen tree – temperate**	13.0	12.5	9.1	10.7
2	**Needleleaf evergreen tree - boreal**	0.0	0.1	0.0	4.9
3	**Needleleaf deciduous tree – boreal**	0.1	0.0	0.0	0.0
4	**Broadleaf evergreen tree – tropical**	0.0	0.0	0.0	0.0
5	**Broadleaf evergreen tree – temperate**	0.0	0.4	1.9	0.0
6	**Broadleaf deciduous tree – tropical**	2.9	0.0	0.0	0.0
7	**Broadleaf deciduous tree – temperate**	1.5	0.4	1.8	1.5
8	**Broadleaf deciduous tree – boreal**	0.0	0.0	0.0	0.3
9	**Broadleaf evergreen shrub - temperate**	21.1	5.3	0.0	0.3
10	**Broadleaf deciduous shrub – temperate**	20.0	37.5	27.4	10.8
11	**Broadleaf deciduous shrub – boreal**	0.9	0.2	0.0	1.0
12	**C_3 arctic grass**	0.0	0.0	1.2	2.2
13	**C_3 grass**	1.0	28.0	14.9	18.9
14	**C_4 grass**	10.4	0.0	0.0	0.0
15	**Crop**	3.2	6.5	4.1	6.3

[1]USGS is the 16-PFT dataset converted from the default 24 USGS land cover dataset based on a lookup table derived from Bonan et al. [1996];
[2]VEG1 is from the PFT fractional cover product by Ke et al. [2012];
[3]VEG2 is obtained from the NCAR CESM data repository [Oleson et al., 2010];
[4]VEG3 is derived from a dataset over the U.S. with 16 PFT classifications by combining the National Land Cover Dataset (NLCD, Homer et al., 2004) and the Cropland Data Layer (see http://nassgeodata.gmu.edu/CropScape/).

Table 2 Experiments of WRF-Chem

	Surface scheme	BVOC scheme	Plant Function Type Dataset				
			USGS/VEG-M	USGS	VEG1	VEG2	VEG3
WRF-Chem	CLM4.0	MEGANv2.0	Mv20CLM	-	-	-	-
		MEGANv2.1	-	Mv21USGS	Mv21V1	Mv21V2	Mv21V3
	Noah	MEGANv2.0	Mv20Noah	-	-	-	-

Geosci. Model Dev. Discuss., doi:10.5194/gmd-2015-266, 2016
Manuscript under review for journal Geosci. Model Dev.
Published: 19 January 2016

Geoscientific Model Development Discussions
Open Access
EGU

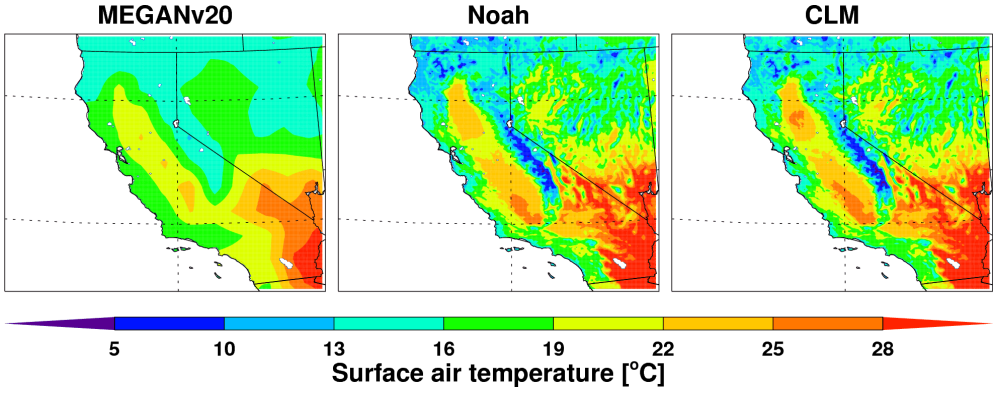

Figure 1 Spatial distributions of monthly mean surface air temperature in June 2010 from the MEGAN v2.0 climatology dataset (MEANv20, prescribed) and the WRF-Chem simulations with the Noah (Noah, simulated) and CLM4 (CLM, simulated) land surface parameterizations.

Geosci. Model Dev. Discuss., doi:10.5194/gmd-2015-266, 2016
Manuscript under review for journal Geosci. Model Dev.
Published: 19 January 2016

1077

1078

1079

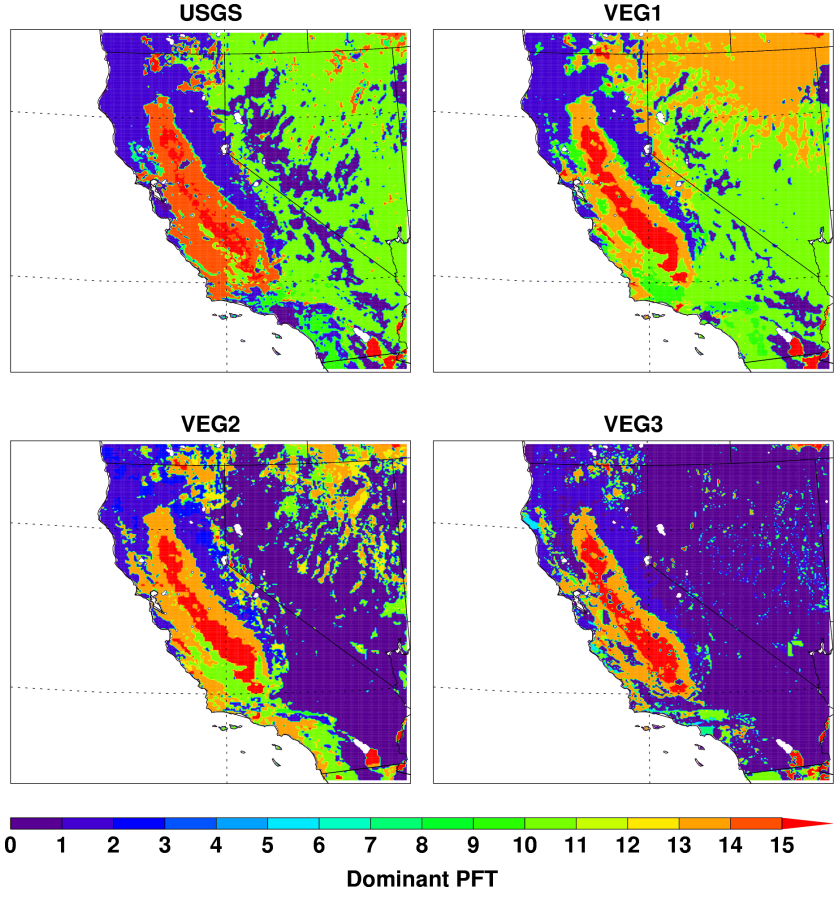

1080

1081 **Figure 2.** Spatial distribution of dominant PFT's over the simulation domain from the
1082 four datasets: USGS, VEG1, VEG2, and VEG3. The PFT number is referred to the list in
1083 Table 1.
1084

1085

1086

1087

Geosci. Model Dev. Discuss., doi:10.5194/gmd-2015-266, 2016
Manuscript under review for journal Geosci. Model Dev.
Published: 19 January 2016

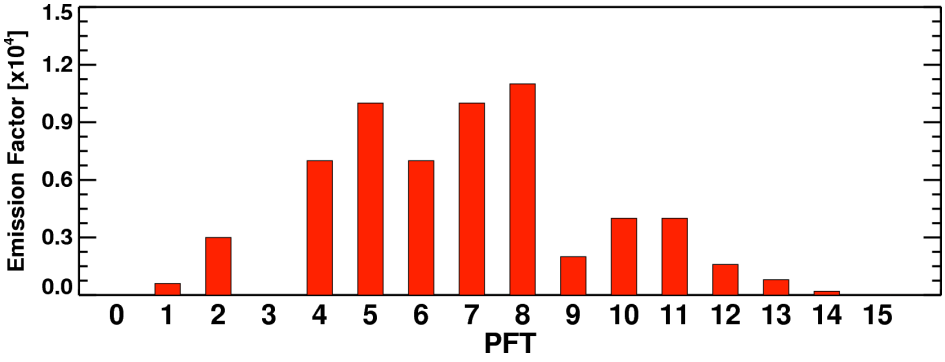

Figure 3. Biogenic isoprene emission factor for each PFT in MEGAN v2.1. The PFT number is referred to the list in Table 1.

Geosci. Model Dev. Discuss., doi:10.5194/gmd-2015-266, 2016
Manuscript under review for journal Geosci. Model Dev.
Published: 19 January 2016

Geoscientific Model Development Discussions
Open Access
EGU

1107

1108

1109

1110

1111

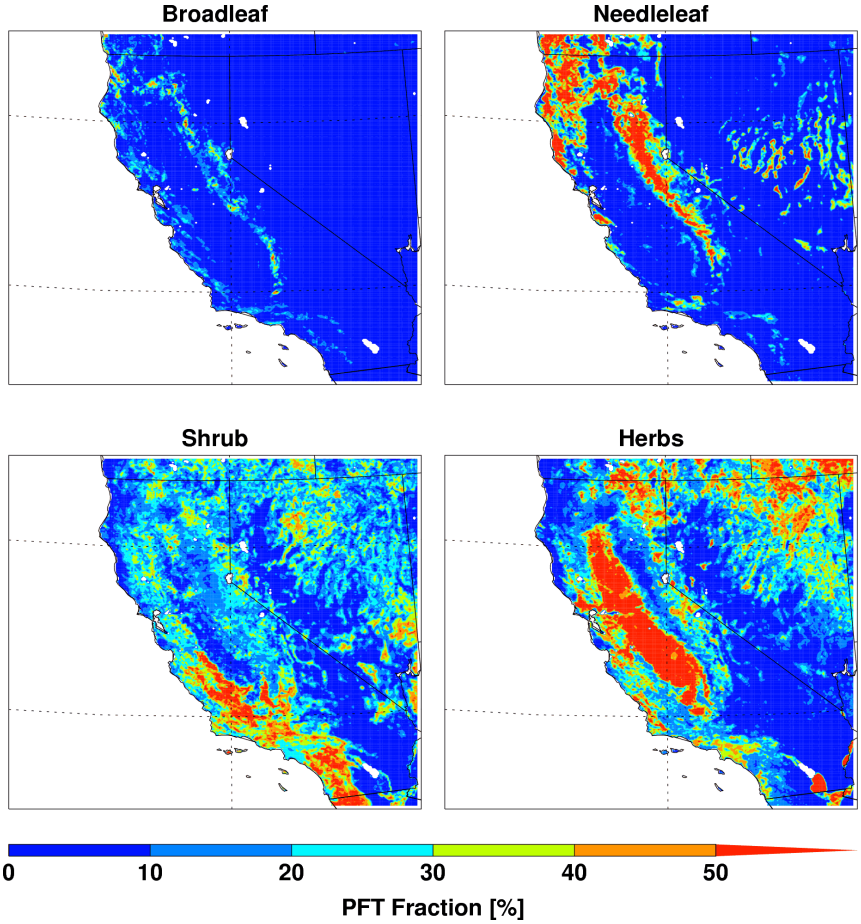

1112
1113 **Figure 4.** Spatial distribution of percentage of the four PFTs from the VEG-M used by
1114 MEGAN v2.0 over the simulation domain.
1115

1116

1117

Geosci. Model Dev. Discuss., doi:10.5194/gmd-2015-266, 2016
Manuscript under review for journal Geosci. Model Dev.
Published: 19 January 2016

Geoscientific Model Development Discussions
Open Access
EGU

1118

1119

1120

1121

1122

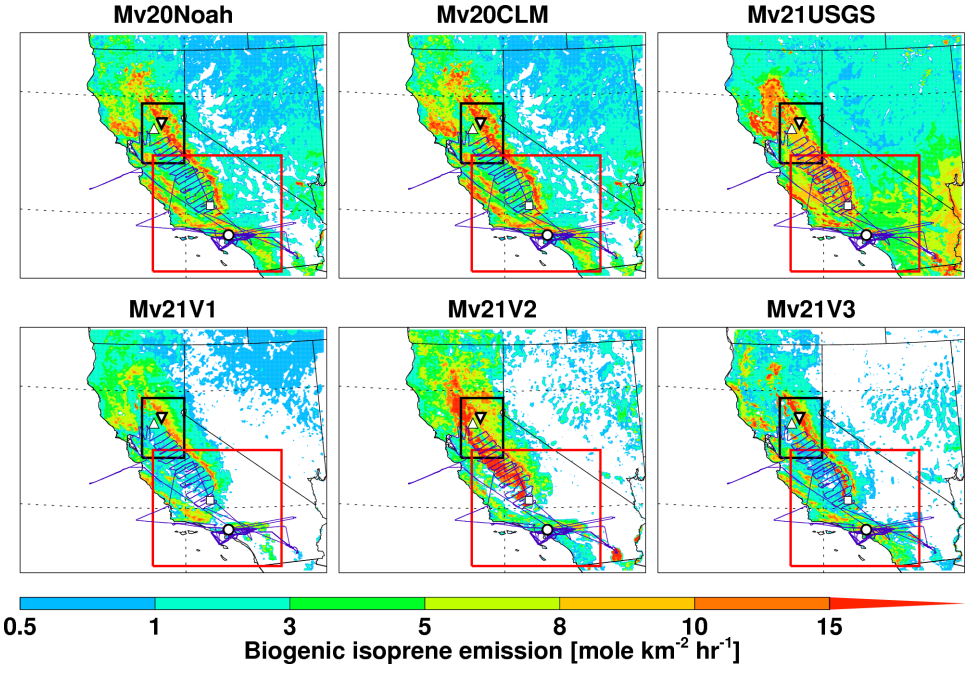

1123

1124 **Figure 5.** Spatial distributions of biogenic isoprene emissions averaged in June estimated
1125 in the six simulations as listed in Table 2. The four observation sites are shown as T0
1126 (white upward triangle), T1 (white downward triangle), Bakersfield (white square), and
1127 Pasadena (white circle). The CalNex WP-3D flight tracks below 1 km (blue line) during
1128 June 2010 are also shown. The black and red boxes denote the predominant CARES and
1129 CalNex regions, respectively.
1130

1131

1132

1133

1134

Geosci. Model Dev. Discuss., doi:10.5194/gmd-2015-266, 2016
Manuscript under review for journal Geosci. Model Dev.
Published: 19 January 2016

Geoscientific Model Development Discussions

1135

1136

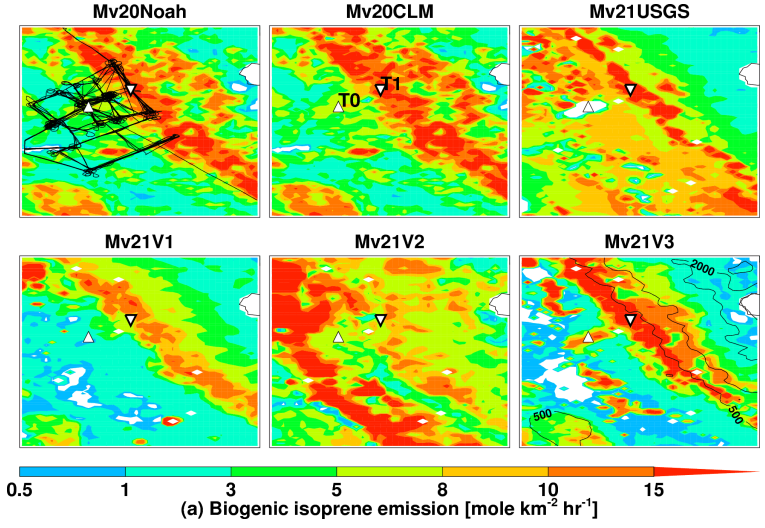

1137

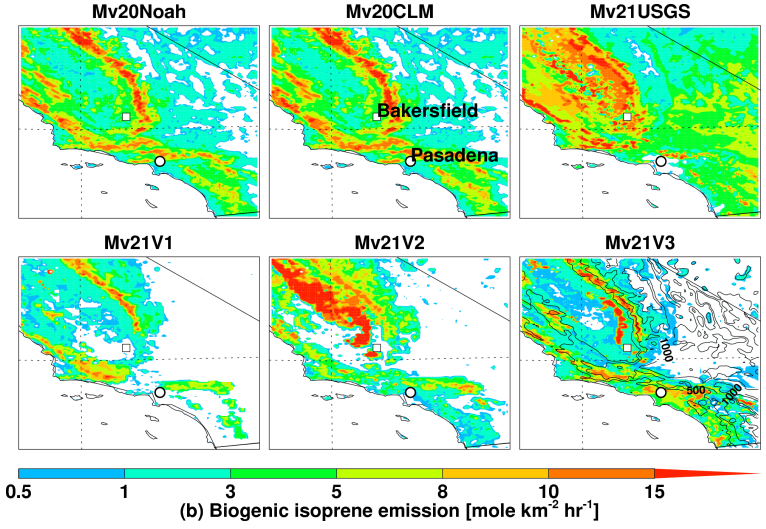

1138

1139 **Figure 6.** a) Spatial distributions of biogenic isoprene emissions around the CARES
1140 observational sites T0 and T1 (the black box shown in Fig. 5) estimated in the six
1141 simulations as listed in Table 1. The CARES G-1 flight tracks below 1 km (black line)
1142 during June 2010 are also shown with the Mv20Noah result; the terrain height is also
1143 shown as the black contour lines with the Mv21V3 result. b) Same as a) except around
1144 the CalNex observational sites Bakersfield and Pasadena (the red box shown in Fig. 5).
1145

Geosci. Model Dev. Discuss., doi:10.5194/gmd-2015-266, 2016
Manuscript under review for journal Geosci. Model Dev.
Published: 19 January 2016

1146

1147

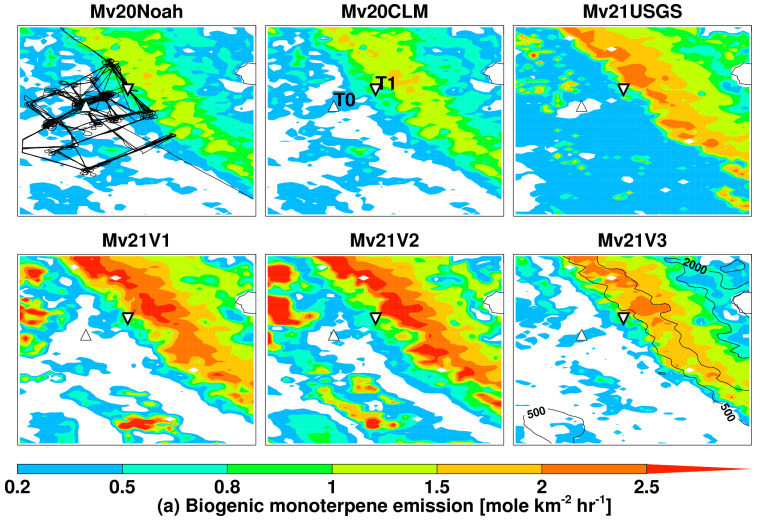

1148

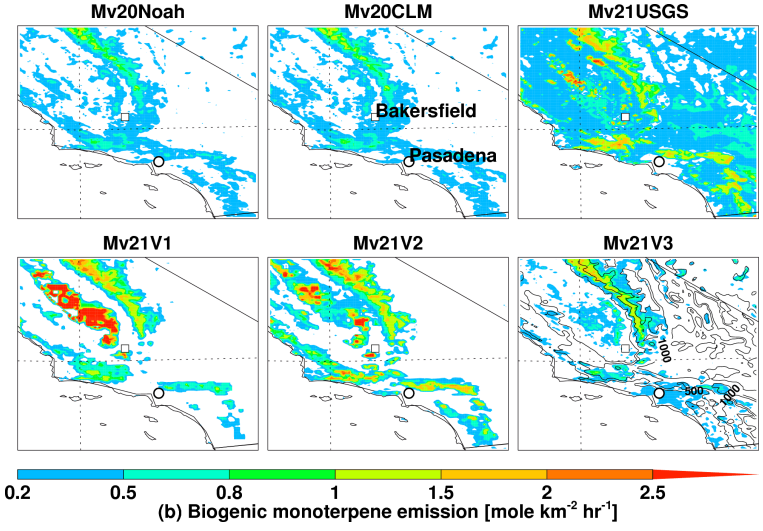

1149

1150 **Figure 7.** Same as Fig. 6, except for biogenic monoterpene emissions.

1151

1152

1153

Geosci. Model Dev. Discuss., doi:10.5194/gmd-2015-266, 2016
Manuscript under review for journal Geosci. Model Dev.
Published: 19 January 2016

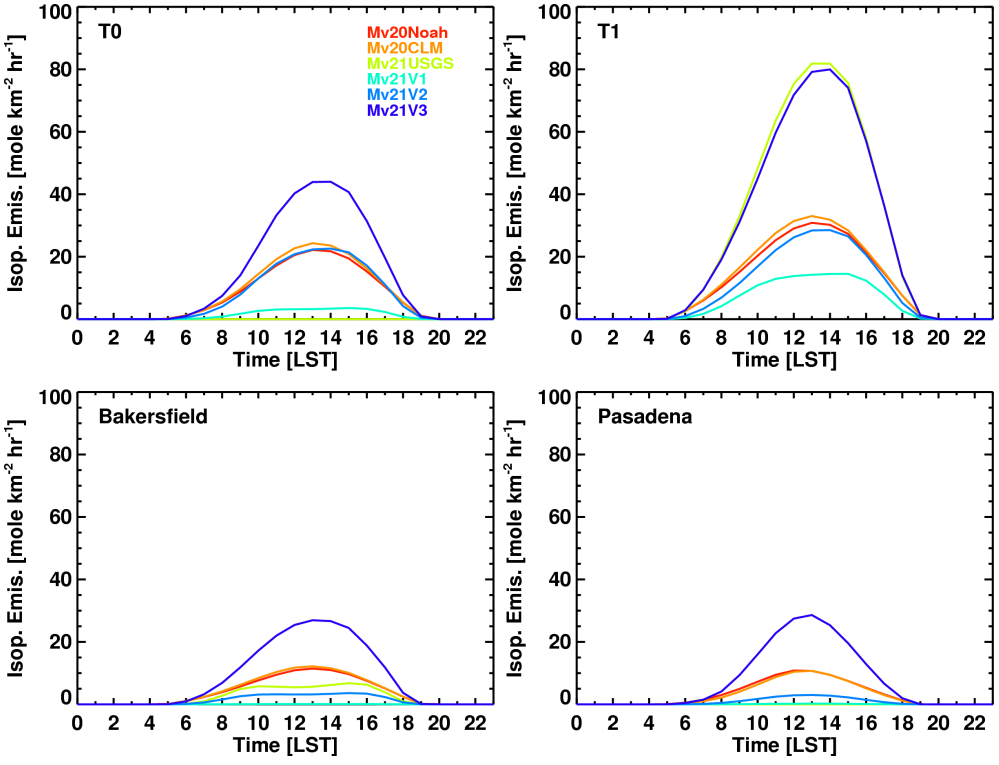

Figure 8. Average diurnal variation of biogenic isoprene emissions at the four observation sites from the six simulations listed in Table 1.

Geosci. Model Dev. Discuss., doi:10.5194/gmd-2015-266, 2016
Manuscript under review for journal Geosci. Model Dev.
Published: 19 January 2016

Geoscientific Model Development Discussions
Open Access
EGU

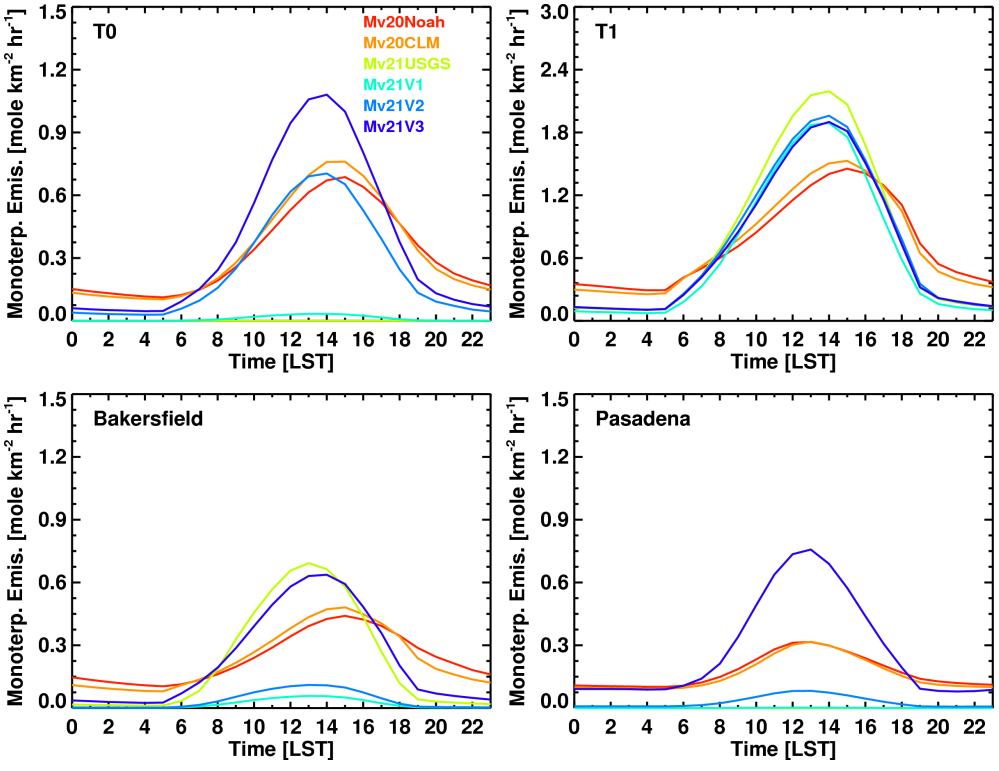

Figure 9. Same as Fig.8, except for biogenic monoterpene emissions.

Geosci. Model Dev. Discuss., doi:10.5194/gmd-2015-266, 2016
Manuscript under review for journal Geosci. Model Dev.
Published: 19 January 2016

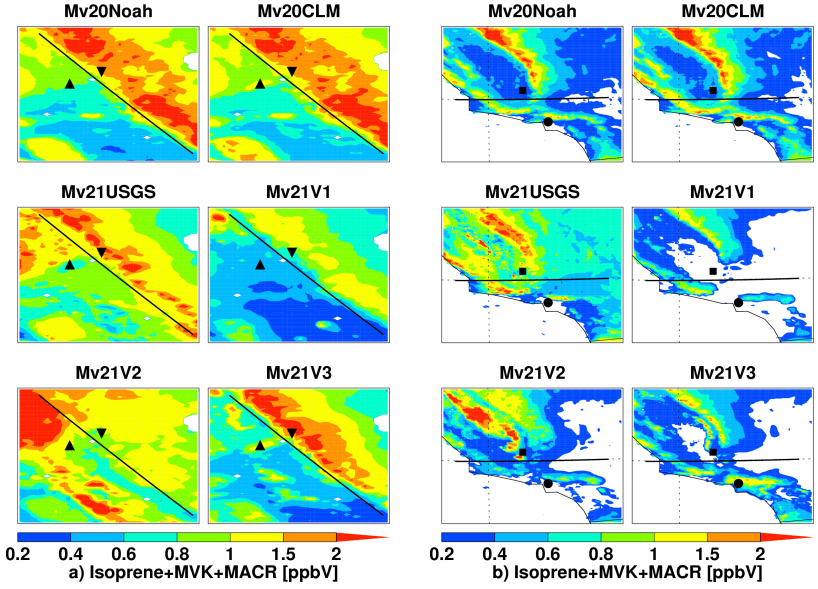

Figure 10. a) Spatial distributions of monthly averaged surface isoprene mixing ratios around the CARES T0 and T1 observational sites from the six simulations as listed in Table 1. The black lines parallel to the Sierra Nevada divide the region to the Southwest and the Northeast for comparison with CARES G-1 aircraft measurements shown in Fig. 14 and 15. b) Same as a) except around the CalNex observational sites Bakersfield and Pasadena. The black lines divide the region to southern California and the Central Valley for comparison with CalNex WP-3D aircraft measurements shown in Fig. 14 and 15.

Geosci. Model Dev. Discuss., doi:10.5194/gmd-2015-266, 2016
Manuscript under review for journal Geosci. Model Dev.
Published: 19 January 2016

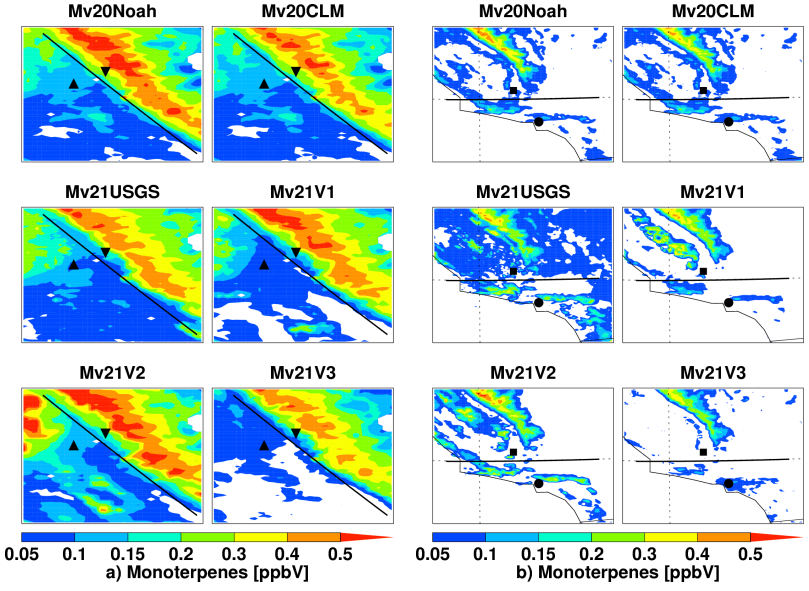

Figure 11. Same as Fig. 10, except for monoterpene.

Geosci. Model Dev. Discuss., doi:10.5194/gmd-2015-266, 2016
Manuscript under review for journal Geosci. Model Dev.
Published: 19 January 2016

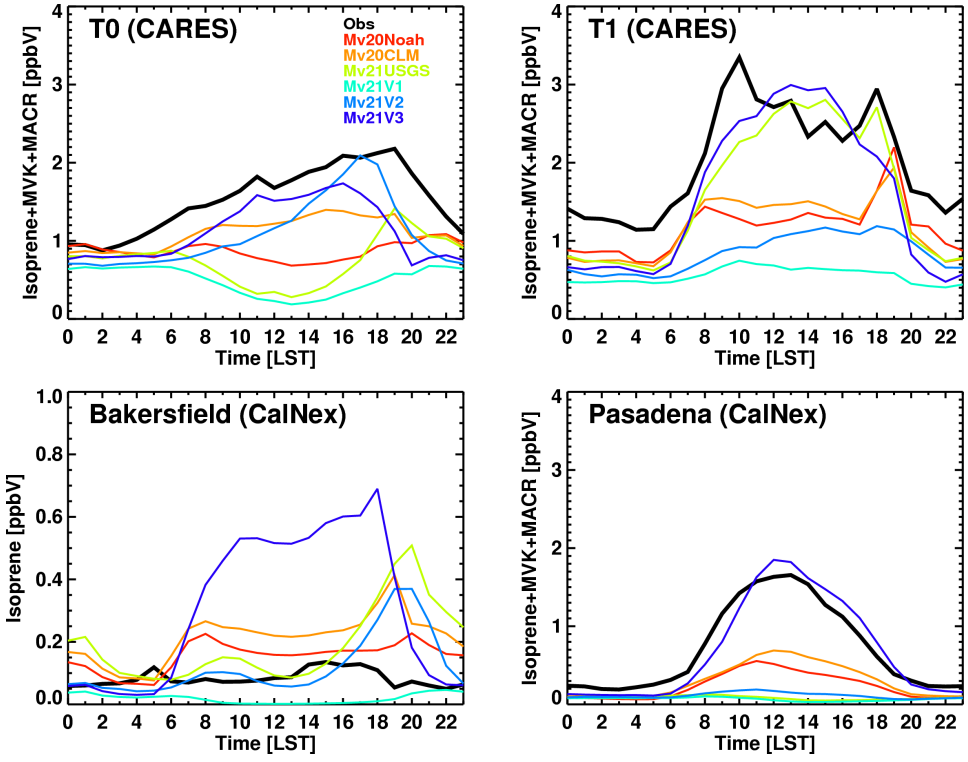

Figure 12. Monthly averaged diurnal variation of surface isoprene mixing ratios at the four observation sites from the observations and six simulations listed in Table 2. The simulated values for the Bakersfield and Pasadena sites are averaged for the first two weeks of June to be consistent with the observations.

Geosci. Model Dev. Discuss., doi:10.5194/gmd-2015-266, 2016
Manuscript under review for journal Geosci. Model Dev.
Published: 19 January 2016

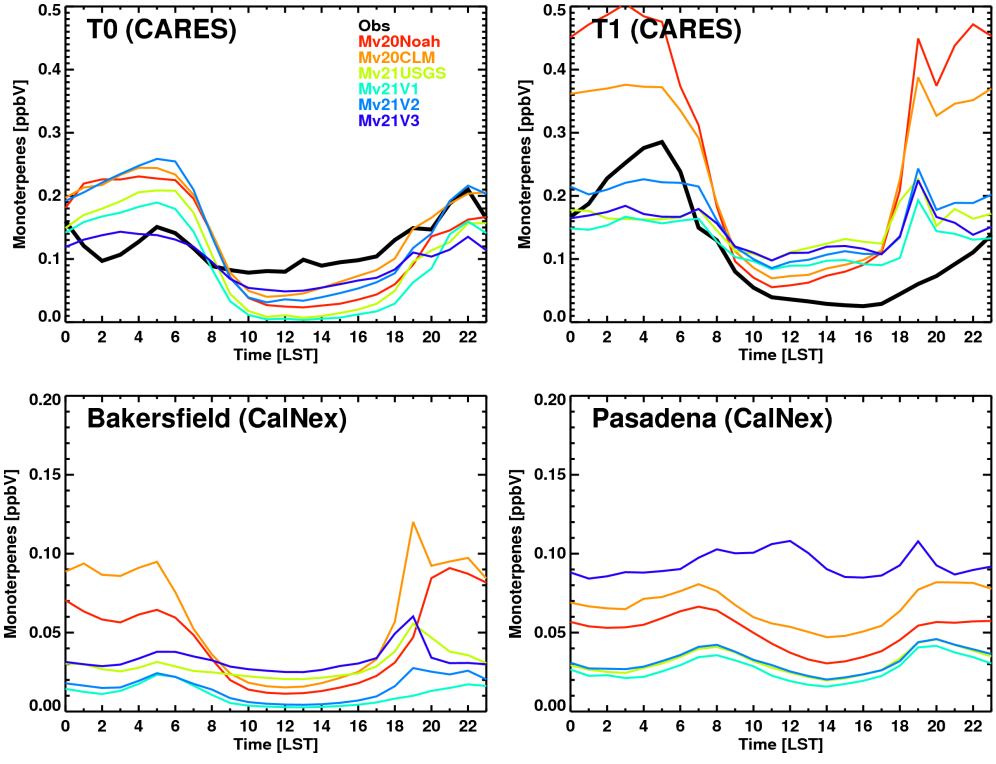

Figure 13. Monthly averaged diurnal variation of surface monoterpene mixing ratios at the four observation sites from the observations and six simulations as listed in Table 2. There are no observations for the Bakersfield and Pasadena sites in June.

Geosci. Model Dev. Discuss., doi:10.5194/gmd-2015-266, 2016
Manuscript under review for journal Geosci. Model Dev.
Published: 19 January 2016

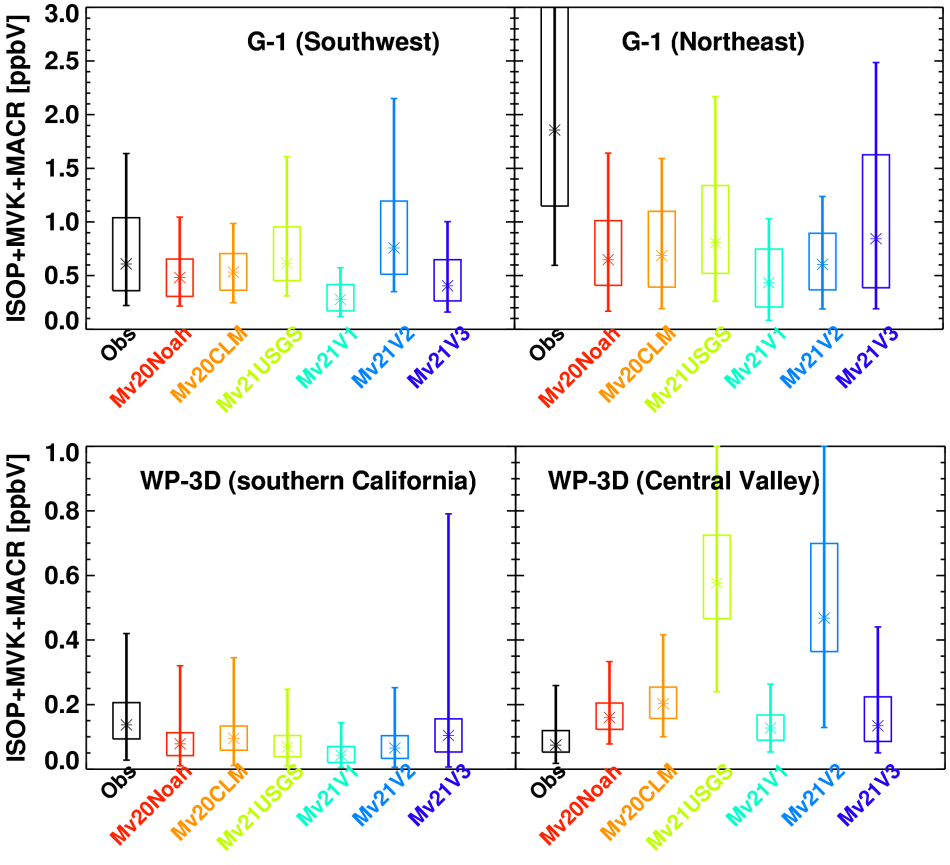

Figure 14. Comparison of isoprene+MVK+MACR mixing ratios averaged below 1 km from the observations by G-1 flights over the Southwest and Northeast regions (as marked in Fig. 10a) and WP-3D flights over southern California and the Central Valley (as marked in Fig. 10b) and the corresponding simulations. Asterisk denotes the 50th percentiles. Vertical lines denote 10th and 90th percentiles, and the boxes denote the 25th and 75th percentiles.

Geosci. Model Dev. Discuss., doi:10.5194/gmd-2015-266, 2016
Manuscript under review for journal Geosci. Model Dev.
Published: 19 January 2016

Geoscientific Model Development Discussions
Open Access
EGU

1250

1251

1252

1253

1254

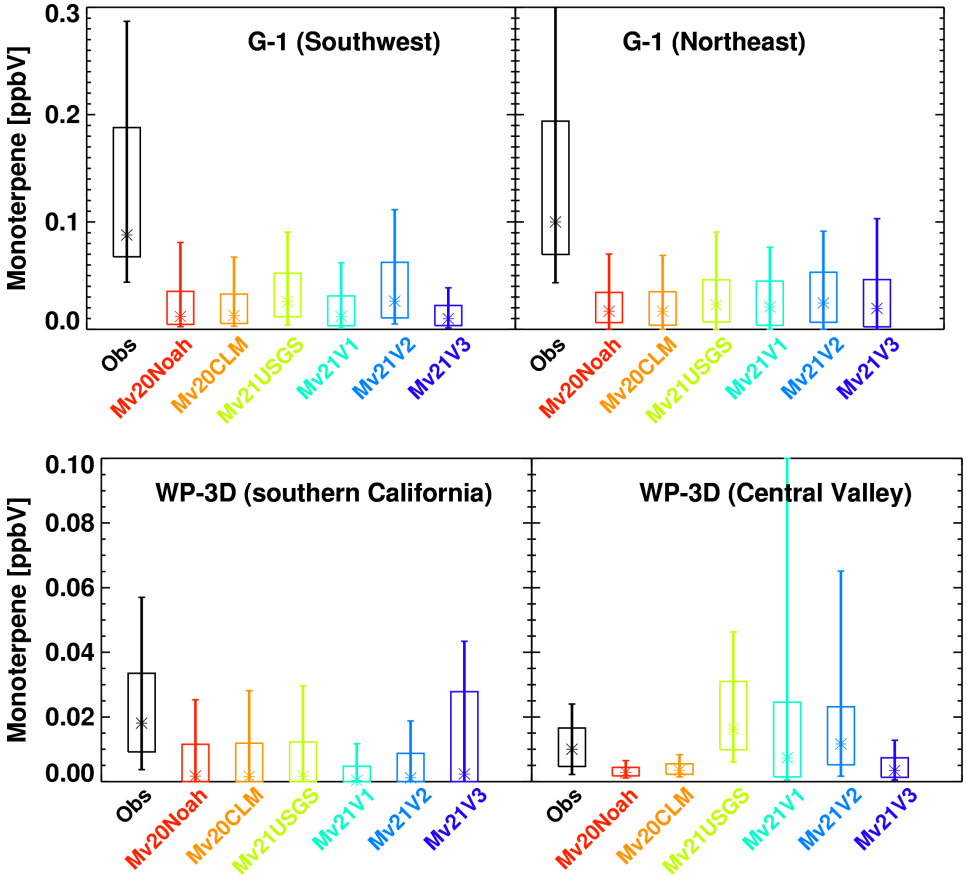

1255

1256

1257 **Figure 15.** Same as Fig. 14 except for monoterpene mixing ratios.

1258